

Accepted Manuscript

Design, synthesis of 4,5-diazafluorene derivatives and their anticancer activity *via* targeting telomeric DNA G-quadruplex

Kang Zhou, Jiachun Liu, Xuqiong Xiong, Mei Cheng, Xiaolin Hu, Suresh Narva, Xiaoyin Zhao, Yanling Wu, Wen Zhang



PII: S0223-5234(19)30529-X

DOI: <https://doi.org/10.1016/j.ejmech.2019.06.012>

Reference: EJMECH 11415

To appear in: *European Journal of Medicinal Chemistry*

Received Date: 8 March 2019

Revised Date: 2 June 2019

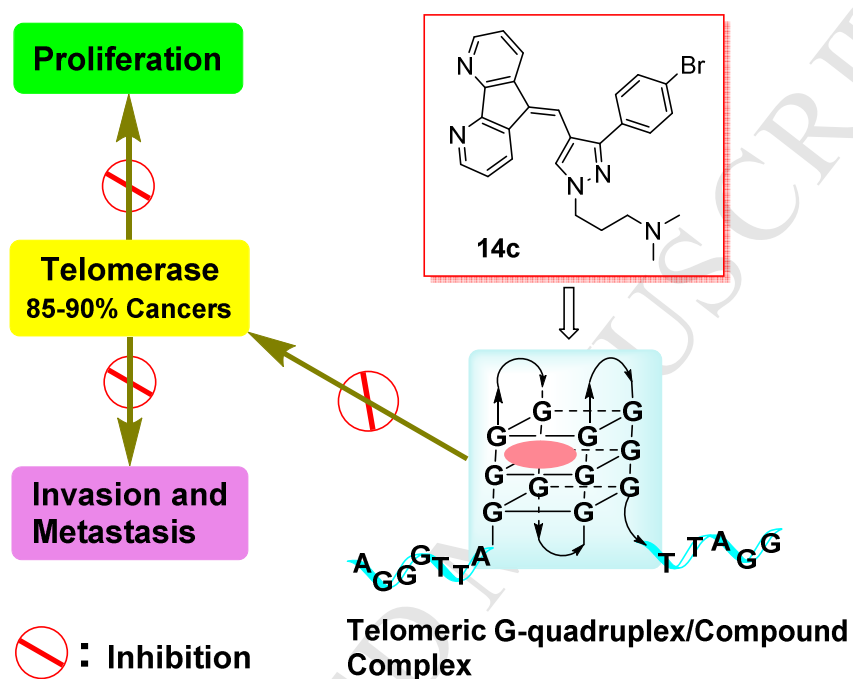
Accepted Date: 3 June 2019

Please cite this article as: K. Zhou, J. Liu, X. Xiong, M. Cheng, X. Hu, S. Narva, X. Zhao, Y. Wu, W. Zhang, Design, synthesis of 4,5-diazafluorene derivatives and their anticancer activity *via* targeting telomeric DNA G-quadruplex, *European Journal of Medicinal Chemistry* (2019), doi: <https://doi.org/10.1016/j.ejmech.2019.06.012>.

This is a PDF file of an unedited manuscript that has been accepted for publication. As a service to our customers we are providing this early version of the manuscript. The manuscript will undergo copyediting, typesetting, and review of the resulting proof before it is published in its final form. Please note that during the production process errors may be discovered which could affect the content, and all legal disclaimers that apply to the journal pertain.

Design, synthesis of 4,5-diazafluorene derivatives and their anticancer activity *via* targeting telomeric G-quadruplex

Kang Zhou^{a,b,1}, Jiachun Liu^{a,b,1}, Mei Cheng^{a,b}, Xiaolin Hu^{a,b}, Suresh Narva^{a,b}, Xiaoyin Zhao^{a,b}, Xuqiong Xiong^{a,b}, Yanli Wang^{a,b}, Yanling Wu^{c,*}, Wen Zhang^{a,b,*}



This kind of 4,5-diazafluorene derivatives with an extended planar aromatic system can interact with the telomeric G-quadruplexes, inhibit the telomerase activity and consequently cancer cells proliferation.

Design, synthesis of 4,5-diazafluorene derivatives and their anticancer activity via targeting telomeric DNA G-quadruplex

Kang Zhou^{a,b,1}, Jiachun Liu^{a,b,1}, Xuqiong Xiong^{a,b}, Mei Cheng^{a,b}, Xiaolin Hu^{a,b}, Suresh Narva^{a,b},
Xiaoyin Zhao^{a,b}, Yanling Wu^{c,*}, Wen Zhang^{a,b,*}

Lab of Chemical Biology and Molecular Drug Design, ^aCollege of Pharmaceutical Science and ^bInstitute of Drug Development & Chemical Biology, Zhejiang University of Technology, Hangzhou, 310014, China.

^cLab of Molecular Immunology, Virus Inspection Department, Zhejiang Provincial Center for Disease Control and Prevention, Hangzhou, 310051, China

*Corresponding author. Lab of Chemical Biology and Molecular Drug Design, College of Pharmaceutical Science, Zhejiang University of Technology, 18 Chaowang Road, Hangzhou, 310014, PR China; Tel: +86-571-88871507; Fax: +86-571-88871507; e-mail: wzhang63@zjut.edu.cn

¹ These authors contributed equally to this work.

Abstract

In our work, 19 novel 4,5-diazafluorene derivatives (**11a-d**, **12a-d**, **13a-d**, **14a-c**, **15c**, **16a-c**) bearing a 1,3-disubstituted pyrazol/thioxothiazolidinone or thioxothiazolidinone-oxadiazole moieties were designed, synthesized, preliminarily explored for their antitumor activities and *in vitro* mechanism. All compounds showed different values of antiproliferative activity against A549, AGS, HepG2 and MCF-7 cell lines through CCK-8. Especially, the compound **14c** exhibited the strongest activity and best selectivity against A549 cells with an IC₅₀ 1.13 μM and an SI value of 7.01 relative to MRC-5 cells, which was better than cisplatin (SI = 1.80) as a positive control. Experimental results at extracellular level demonstrated that compounds **14a-c** could strongly interact with the G-quadruplex(es) formed in a 26nt telomeric G-rich DNA, in particular, the **14c** exhibits quite strong binding affinity with an association equilibrium constant (K_A) of 7.04(±0.16) × 10⁷ M⁻¹ and more than 1000-fold specificity to G4-DNA over ds-DNA and Mut-DNA at the compound/G4-DNA ratio of 1:1. Further trap assay ascertained that compounds **14a-c** owned strong inhibitory ability of telomerase activity in A549 cells, suggesting that these compounds have great possibility to target telomeric G-quadruplexes and consequently indirectly inhibit the telomerase activity. In addition, it is worthy of note that the remarkable inhibitory effects of **14a-c** on the mobility of tested cancer cells were observed by wound healing assays. Furthermore, molecular docking and UV-Vis spectral results unclose the rationale for the interaction of compounds with such G-quadruplex(es). These results indicate that the growth and

metastasis inhibition of cancer cells mediated by these 4,5-diazafluorene derivatives possibly result from their interaction with telomeric G-quadruplexes, suggesting that 4,5-diazafluorene derivatives, especially **14c**, possess potential as anticancer drugs.

Keywords: 4,5-diazafluorene, telomeric G-quadruplex, telomerase activity, cancer cells, antiproliferative activity

1. Introduction

Cancer morbidity and mortality are rapidly growing worldwide and cancer has become a serious public health problem. The report of GLOBOCAN 2018 estimates on cancer indicates that there will be 18.1 million new cases of cancer and 9.6 million deaths occurred from cancer in 2018 [1]. Especially, it is estimated that the cancer morbidity and mortality rates are high in China, rank the top one in the world, accounting for over one-fifth of the new cancer cases and cancer deaths occurred in the world in 2018. In both sexes combined, lung cancer is the most commonly diagnosed cancer (11.6% of the total cases) and the leading cause of cancer death (18.4% of the total cancer deaths). It is noteworthy that non-small cell lung carcinomas (NSCLC) accounts for about 85% of all lung cancers. NSCLCs are relatively insensitive to chemotherapy, compared to small cell carcinoma. The mortality rate of NSCLC patients remains high with relapse, the five-year survival rate in stages I through IV significantly decreases due to the advancement of the disease and is 47% for stage I, 30% for stage II, 10% for stage III, and 1% for stage IV [2–5]. In addition, breast cancer is the most familiar malignancy among women. Over the past decade, the number of breast cancer cases has been rising. According to statistics, there are 2.08 million new breast cancer cases, approximately 11.6% of all newly diagnosed cancer cases in 2018 [1]. Gastric cancer is still the third most common worldwide malignant tumor disease; there exists a high regional difference in its morbidity. Especially in developing countries, the morbidity of gastric cancer is high, estimated to account for about 8% of all new cases of cancer, the number of new cases will rise to 1.7 million cases by 2030 [6,7]. Hepatocellular carcinoma (HCC), one of the most common malignancies in the world, is the third leading cause of cancer death, the morbidity of HCC, which was highest in Asia and sub-Saharan Africa, has increased in Western countries [8]. It was reported that 0.841 million new liver cancer cases each year occurred in both men and women, with the mortality rate increased to 10.2% and

5.6% respectively [1]. Collectively, various data indicate that cancer is a huge threat to human health and a great challenge to medical research.

In recent years, a variety of clinical anticancer strategies (eg. chemotherapy, radiotherapy and surgical resection) have been enduring to develop and progress. These treatments can alleviate the symptoms of patients to a certain extent, but some cancers cannot be completely cured by these therapies, the overall 5-year survival rate of patients is still very low. There are also a number of disadvantages that cannot be ignored, such as patient compliance, side effects of radiotherapy and chemotherapy, limitations of surgical resection, cell resistance, etc. These problems should be responsible for the low survival rate of the patients. Therefore, the new target therapy agents that highly effectively and preferentially induce apoptosis of cancer cells rather than normal cells will bring hopes for the future.

On the other hand, telomerase shows dynamic activity in 85-90% cancer cells. Telomerase can maintain the length of telomere as well as promote the process of cell cycle, so that the cancer cells endow more vitality and avoid apoptosis in process of cell proliferation, while it is also associated with the invasion and metastasis of cancer cells [9–13]. Hence, inhibition of the telomerase activity may be a novel strategy for cancer chemotherapy. Special DNA sequences containing $(TTAGGG)_n$ repeats in human telomeres [14–16] can fold into G-quadruplex (G4-DNA) structures under approximate physiological conditions, which can effectively inhibit the activity of telomerase and promote apoptosis [17–19], as depicted in **Fig. 1**. In addition, studies have found that telomeric G4-DNA ligands can trigger telomere dysfunction and DNA damage response, thereby inducing cellular senescence or apoptosis [20]. At the same time, with the study of G-quadruplex probes, the dynamic folding and unfolding of G4-DNA can be traced and this lays a foundation for further research [21–23]. Therefore, the telomeric G4-DNA ligands have great potential to be developed as new target agents for the treatment of cancers.

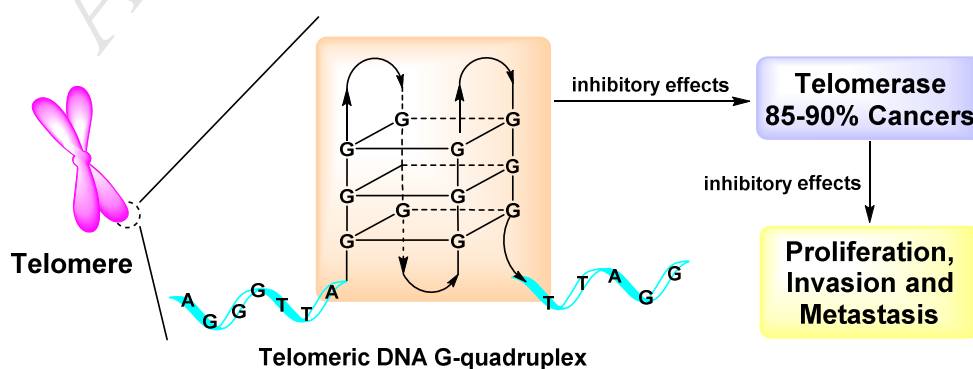
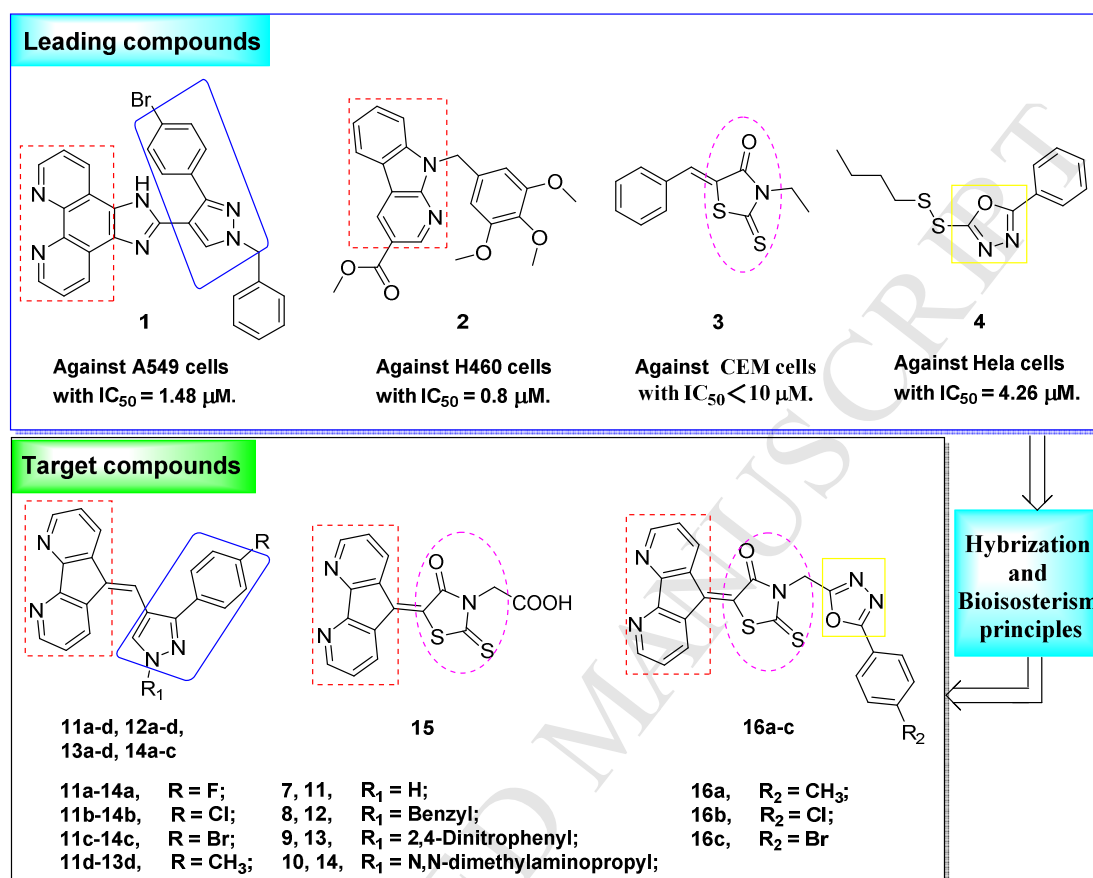


Fig. 1. The effects of telomerase on the proliferation, invasion and metastasis of cancer cells and development of telomerase targeted drugs mediated by formation and stabilization of DNA G-quadruplex.



Scheme 1. Structure of the leading compounds and design strategy of the target compounds.

In our previous work [24], the phenanthroline derivative **1** (**Scheme 1**) exhibited potential antiproliferative activity against A549 cell line with the half maximal inhibitory concentration (IC_{50}) of $1.48 \mu M$ and also showed significant inhibitory effect on the growth, migration of A549 cells by its possible interaction with telomeric DNA to stabilize G4-DNA structure to some extent. However, the compound **1** had some defects that cannot be ignored, such as poor solubility, weak stability to telomeric G4-DNA and inferior selectivity to cancer cells. This implied that the compound **1**, acting as a stabilizer of telomeric G-quadruplex, needs further structural modification as a leading compound to develop cancer inhibitors. The another compound **2** (**Scheme 1**), a kind of α -carboline derivatives, showed high levels of cytotoxicity against HL-60, COLO 205, Hep3B, and H460 cells with IC_{50} values of 0.30, 0.49, 0.70, and 0.80 μM respectively [25]. Based on these previous findings, it is worthwhile to study whether the

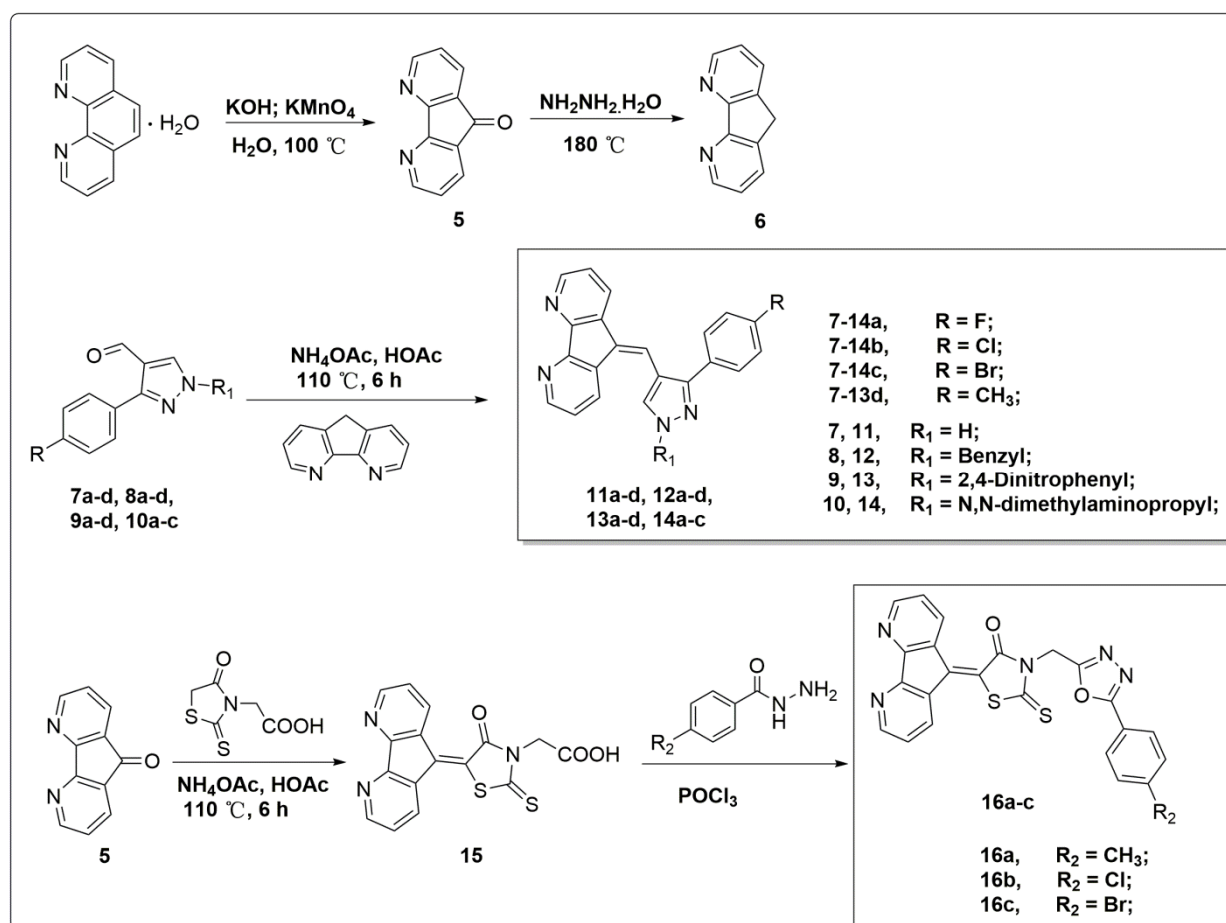
bioisostere structure (4,5-diazofluorene) of the carbazole and phenanthroline structures has the better antitumor activity or not. Simultaneously considering too strong rigid conjugate plane of 1*H*-imidazo[4,5-*f*][1,10]phenanthroline skeleton bearing a pyrazole moiety designed in previous work [24], possibly leading to their interaction instability and weak interaction with target DNA's and inferior cell selectivity, using a combination of bioisosterism principle using compounds **1** and **2** as the leading compounds, we designed, synthesized fifteen novel compounds (**11a–d**, **12a–d**, **13a–d**, **14a–c**) bearing a 1,3-disubstituted pyrazol moiety by substitution of the 1*H*-imidazo[4,5-*f*][1,10]phenanthroline skeleton with a 4,5-diazofluorene skeleton (**Scheme 1**) and evaluated their antitumor activity. On the other hand, rhodanine derivatives with a wide range of biological activities, such as antibacterial [26], antiviral [27], antitumor [28] and lower blood glucose [29], have already attracted plenty of attention. Compound **3** (**Scheme 1**) showed significant antitumor activity against CEM cells with an IC₅₀ value of less than 10 μM, indicating that the rhodanine moiety of the compound played a key role in antitumor property [30]. In addition, 1,3,4-oxadiazole is a privileged scaffold incorporated in many compounds presenting potent antitumor activity. Compound **4** displayed highly effective inhibitory activity against Hela cells with an IC₅₀ value of 4.26 μM [31]. Likewise, based on combination principle, other four novel compounds (**15**, **16a–c**) (**Scheme 1**) bearing a thioxothiazolidinone or thioxothiazolidinone-oxadiazole moieties were designed, synthesized and evaluated for their antitumor activity.

2. Results

2.1 Chemistry

The synthetic route of the 4,5-diazafluorene derivatives **11–16** is depicted in **Scheme 2**. Compounds **5**, **6**, **7a–d**, **8a–d**, **9a–d**, **10a–c**, 2-(4-oxo-2-thioxothiazolidin-3-yl)acetic acid and 4-substituted benzohydrazides were reported in a previous paper [24,32–35]. Compounds **11a–d**, **12a–d**, **13a–d**, and **14a–c** were synthesized through the Knoevenagel reaction by heating a mixture of compound **6** and **7a–d**, **8a–d**, **9a–d**, **10a–c** in the presence of ammonium acetate and glacial acetic acid at 110 °C for 6 h. Compound **15** was synthesized through the Knoevenagel reaction, then **15** was subjected to the condensation reaction with 4-substituted benzohydrazides under phosphorus oxychloride condition (105 °C) for 5 h to obtain compounds **16a–c**. The

structures of the synthesized compounds were confirmed by ^1H NMR, ^{13}C NMR and Mass spectral analysis.



Scheme 2. Synthesis of 4,5-diazafluorene target compounds **11–16**.

2.2 *In vitro* anti-tumor activity evaluation by CCK-8 assay

To evaluate the antiproliferative abilities of novel synthesized compounds **11–16** against A549 cells, AGS cells, HepG2 cells, MCF-7 cells and MRC-5 cells (normal human fetal lung fibroblast cells as a reference) by Cell Counting Kit-8 technique [24], initially, four kinds of cancer cells were exposed to 10 μM of compounds **11–16** for 36 h, respectively and the progressive cell growth inhibition observed. As shown in **Fig. 2A** and **Fig. S1**, all the synthesized derivatives presented different values of antiproliferative activity against all tested cancer cells. In particular among all compounds, three compounds **14a–c** exhibited the most potent activity at 10 μM , which was stronger than that of cisplatin as a positive control. Secondly, as shown in **Fig. 2B**, **2C**, **2D**, **2E** and **Table 1**, after four kinds of cancer cells were treated with two-fold serial

dilution of **14a–c** and cisplatin for 36 h, it was found that **14a–c** exhibited potent activity against all tested cancer cells with IC_{50} values ranging from 1.13 μ M to 11.77 μ M. More notably, the **14c** possessed the best antiproliferative activity with IC_{50} values of $1.13 \pm 0.02 \mu$ M, $1.81 \pm 0.10 \mu$ M, $5.27 \pm 0.07 \mu$ M against A549, AGS, MCF-7 cells respectively, and the strongest inhibitory effect on A549 cells among all the tested four cancer cells. Furthermore, **14c** displayed stronger inhibitory activity than cisplatin with IC_{50} values of $11.90 \pm 0.26 \mu$ M, $3.33 \pm 0.01 \mu$ M, $6.89 \pm 0.17 \mu$ M, respectively, and other similar structural tested compounds **14a, b** at each of 1, 2 and 4 μ M against A549 cells, AGS cells, MCF-7 cells but HepG2 cells.

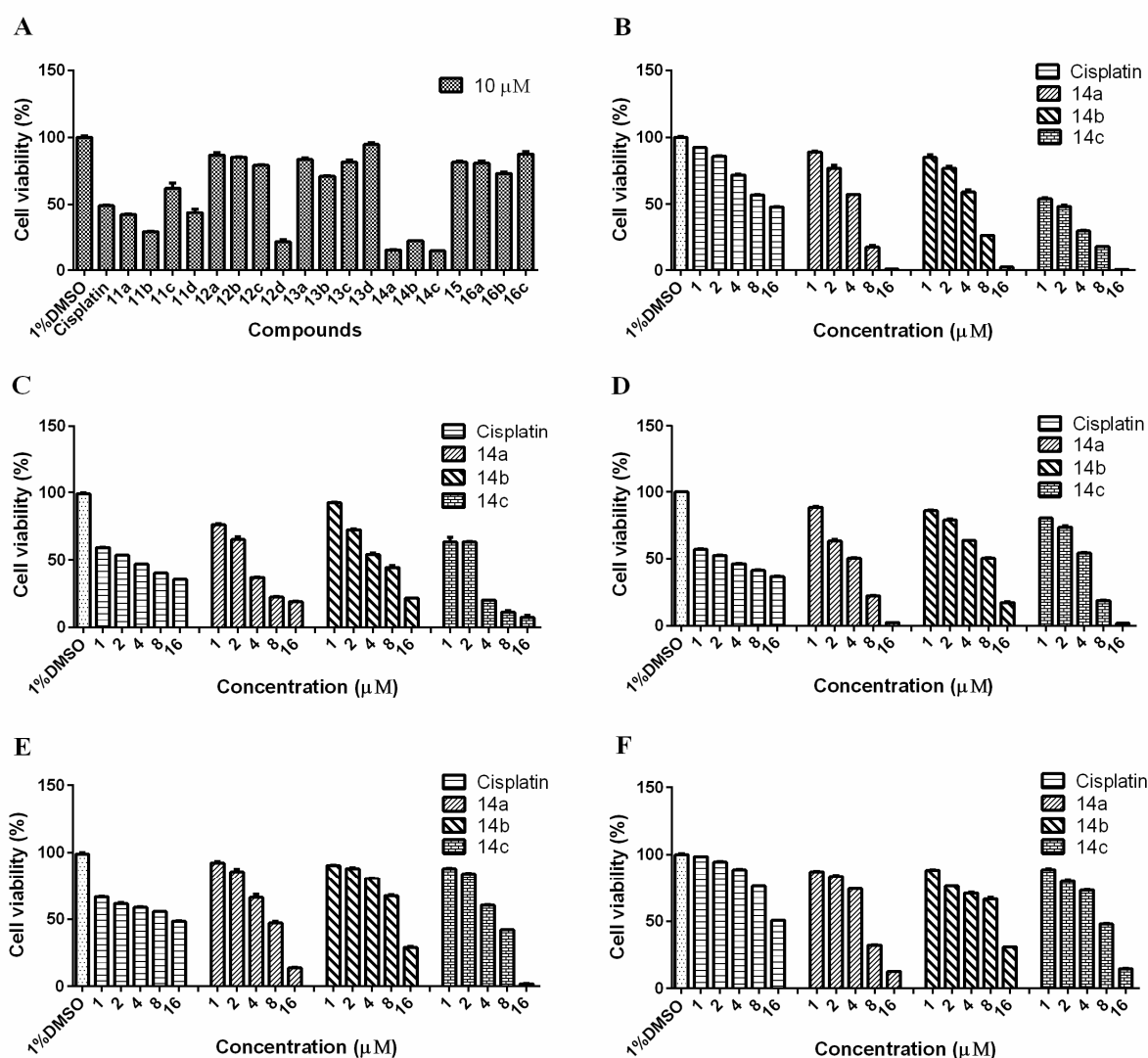


Fig. 2. Viability of A549 cells treated with 10 μ M of compounds **11–16** (A), and A549 cells (B), AGS cells (C), HepG2 cells (D), MCF-7 cells (E), and MRC-5 cells (F) treated with compounds **14a–c** with 0, 1, 2, 4, 8 and 16 μ M for 36 h, respectively. Cell viability was determined using Cell Counting Kit-8 assay. Cisplatin: positive control; 1% DMSO is 1% DMSO solution in RPMI 1640 as a reference.

Also, as shown in **Fig. 2F** and **Table 1**, after the treatment of MRC-5 cells with **14a–c** and cisplatin as a positive control, cytotoxicity results were obtained. The compounds **14a–c** presented moderate cytotoxicity against normal MRC-5 cells with IC_{50} values in the range of 5.93–9.81 μ M, which are 1.72–7.01-fold higher than those of A549 cells. Among compounds **14a–c**, **14c** presented the strongest cytotoxicity against A549 cells over against normal MRC-5 cells with a biggest selectivity-index (SI) value of 7.01 and also showed better selectivity than cisplatin with an SI value of 1.80.

Taken together, all these outcomes suggest that the derivatives **14a–c** showed strong cytotoxicity against four tested cancer cells, especially A549 cells, and **14c** possessed strongest inhibitory activity and best selectivity for A549 cells, implying that **14c** may be explored as a promising A549 cell inhibitor.

Table 1.

IC_{50} values (μ M) for the A549, AGS, HepG2, MCF-7, and MRC-5 cell lines treated with the desired compounds **14a–c** and a positive control drug (cisplatin). The values are expressed as the mean \pm SD (triplicates).

Cancer cells	Cisplatin	14a	14b	14c
A549	11.90 \pm 0.26 (1.80) ^b	3.44 \pm 0.10 ^a (1.72)	4.15 \pm 0.14 ^a (2.36)	1.13 \pm 0.02 ^a (7.01)
AGS	3.33 \pm 0.01 (6.42)	2.93 \pm 0.12 (2.02)	5.52 \pm 0.20 (1.78)	1.81 \pm 0.10 (4.25)
HepG2	3.26 \pm 0.07 (6.56)	3.32 \pm 0.04 (1.79)	6.43 \pm 0.13 (1.52)	3.48 \pm 0.08 (2.21)
MCF-7	6.89 \pm 0.17 (3.10)	6.70 \pm 0.27 (0.88)	11.77 \pm 0.29 (0.83)	5.27 \pm 0.07 (1.46)
MRC-5	21.39 \pm 0.29	5.93 \pm 0.09	9.81 \pm 0.34	7.92 \pm 0.15

^a Statistically different to lung cancer cell line (A549 and MRC-5) ($P < 0.05$).

^b Selectivity-Index

2.3 Interpretation of interaction mechanism of the novel compounds with the target(s) by electrophoretic mobility shift assay (EMSA)

In order to explore whether the novel 4,5-diazafluorene derivatives with moderate conjugated planar aromaticity can induce the formation and stabilization of telomeric G-quadruplexes (G4-DNA's) and consequently mediate the cancer cell apoptosis. We first carried out electrophoretic mobility shift assay (EMSA) at the extracellular molecular level. The sequences of newly designed 26nt telomeric DNA's as target(s) in this experiment for the examination of G4-DNA formation were listed in **Table 2**, containing a Tel26nt G-rich DNA (G-

rich DNA) with four three-guanine repeats ((GGGTTA)₄) which may form G4-DNA's, a complementary strand of Tel26nt C-rich DNA (C-rich DNA), a Tel26nt double-stranded DNA (ds-DNA), and a Tel26 mutated single-stranded DNA (Mut-DNA) with a single G-to-C mutation completely impossible to form any G4-DNA structures under our experimental conditions (a Tris buffer containing 10 mM Tris-HCl, 10 mM KCl, 0.1 mM EDTA, pH = 7.4). To measure the ability of **14a-c** and **16c**, which contains a rhodamine moiety and the same *p*-bromophenyl group as **14c** with strong inhibitory activity and possesses poor cytotoxicity to four examined cancer cells, to induce the formation of and stabilize G4-DNA's from the 26nt telomeric DNA sequences, the properties of electrophoretic mobility shift for tested oligonucleotides treated with a serial dilution of compounds were observed by using a Bio-Rad imaging detector (**Fig. 3** and **Fig. S2A**).

Table 2.

The sequences of DNA oligomers used in this study.

DNA oligomers	DNA sequences
Tel26nt G-rich DNA (G-rich DNA)	5'-TTAGGGTTAGGGTTAGGGTTAGGGTT-3'
Tel26nt C-rich DNA (C-rich DNA)	5'-AATCCCAATCCCAATCCCAATCCCAA-3'
Tel26nt mutated single-stranded DNA (Mut-DNA)	5'-TTAGCGTTAGCGTTAGCGTTAGCGTT-3'
Tel26nt double-stranded DNA (ds-DNA)	5'-TTAGGGTTAGGGTTAGGGTTAGGGTT-3' 3'-AATCCCAATCCCAATCCCAATCCCAA-5'
5'-biotin-G-rich DNA	5'-biotin-TTAGGGTTAGGGTTAGGGTTAGGGTT-3'
5'-biotin-Mut-DNA	5'-biotin-TTAGCGTTAGCGTTAGCGTTAGCGTT-3'
5'-biotin-ds-DNA	5'-biotin-(TTAGGG) ₄ TT-TATA-AA(CCCTAA) ₄ -3'

As shown in **Fig. 3**, at least two kinds of G4-DNA conformations are formed in G-rich DNA alone under our experimental conditions in gels, one for migrating faster and darker band is attributable to an intramolecular G-quadruplex [36] and the other for migrating slower and very faint band possibly ascribed to intermolecular G4-DNA's, and(or) higher order structures relative to a DNA Marker alone on Lane 1 in gel [36-43], but precise molecular structures should be further interpreted by other high-resolution techniques such as nuclear magnetic resonance (NMR) and X-ray crystallography. With increasing concentration of **14a-c** and **16c**, the faster-moving species gradually decreased in a compound concentration-dependent manner and its decreased amount and rate were different with addition of different compounds; among them, the change upon addition of **14c** was most noticeable and that upon addition of **16c** a little. The

slower-moving bands near 20bp, possibly being a mixture of intermolecular G4-DNA's, higher order structures and(or) compound/G4-DNA compounds, greatly changed in the presence of **14a–c** and **16c**, relative to bands of G-rich DNA alone. However, as seen in **Fig. 3**, the species of both slower and faster-moving bands gradually were converted to other some complicated products with addition of more compounds **14a–c** ($\geq 3 \mu\text{M}$), which possibly contain several species of higher order structures and(or) compound/G4-DNA's complexes [38,43], whereas no such change for **16c** was observed. In particular, **14c** at the concentration of $12 \mu\text{M}$ could completely convert the faster-migrating species to less lower-migrating ones near 20bp and more smearing species of higher order structures and(or) compound/G4-DNA's complexes. These data strongly suggest that the examined compounds could differentially interact with 26nt telomeric G4-DNA's to form novel higher order structures and(or) compound/G4-DNA complexes and convert original DNA structural species in the absence of compounds to the slower-migrating ones, with an order of compounds exhibiting strongest such ability to induce the formation of and stabilize G4-DNA structures: **14c**>**14a**>**14b**>**16c**, which is in accord with the results at cellular level by CCK-8 assay.

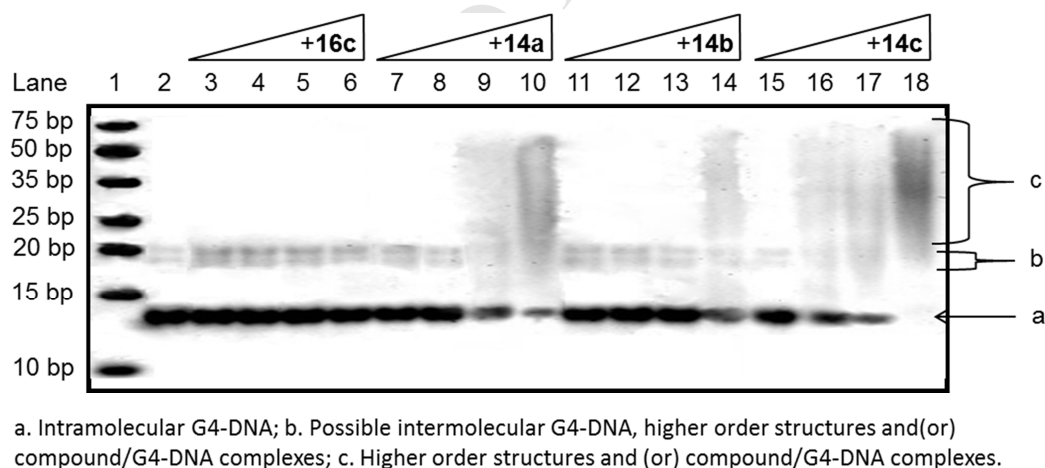


Fig. 3. The ability of four 4,5-diazafluorene derivatives **14a–c** and **16c** to promote the formation of G4-DNA structures by EMSA in a 26nt telomeric single-stranded DNA sequence (G-rich DNA). Lane 1: DNA Marker alone; Lane 2: G-rich DNA alone in 1% DMSO containing buffer; Lane 3-6: G-rich DNA + compound **16c**; Lane 7-10: G-rich DNA + compound **14a**; Lane 11-14: G-rich DNA + compound **14b**; Lane 15-18: G-rich DNA + compound **14c**. Final concentration of DNA's is $2 \mu\text{M}$ for single-stranded DNA (in single strand); the increasing concentration of each compound is $1.5, 3, 6$ and $12 \mu\text{M}$ from left to right.

In addition, as shown in **Fig. 2S**, the mobility properties of three kinds of DNA's: C-rich DNA, Mut-DNA, ds-DNA as negative oligonucleotides, and a 26nt telomeric G-rich RNA

sequence, (UUAGGG)₄UU, were also observed in the presence and absence of **14c** with strongest affinity to G4-DNA. Results indicated that **14c** had no influence on bands for C-rich DNA, Mut-DNA and G-rich RNA, only a bit influence on ds-DNA at a higher concentration of 24 μ M which is the two-fold concentration maximally used in the experiment in **Fig. 3**. Interestingly, based on the moving position of bands for the C-rich DNA relative to the Marker, it was supposed that it adopted a freedom coil form, not a completely linear form under our experimental conditions. Collectively, these results demonstrate at extracellular molecular level that 4,5-diazafluorene derivatives **14a–c** and **16c**, especially **14a–c**, could specifically bind to the 26nt telomeric G4-DNA and induce the conversion between species of and stabilize telomeric G4-DNA structures.

2.4 T_m values for telomeric G-quadruplexes in the presence/absence of 4,5-diazafluorene derivatives

Melting curves are widely used to determine thermodynamic properties of folded nucleic acid/protein structures including their stability and interaction with ligands [44,45]. The melting temperature (T_m , °C), which is the mid-point of a melting curve at which the examined molecular structures is 50% unfolded, is an important parameter to indicate the stability of examined nucleic acid/protein structures in the presence/absence of ligands. Generally, the melting curve with a standard forward “S” type for duplex nucleic acids and one with a standard inverted “S” type for G4-DNA’s are measured due to hyperchromicity at 260 nm [46] and hypochromicity at 295 nm [47], respectively. Thus, in order to assess binding affinity of **14a–c** and **16c** with G-rich DNA’s, we measured melting curves in the presence/absence of 4,5-diazafluorene derivatives **14a–c** and **16c** by monitoring the UV absorbance of the G-rich DNA (**Table 2**) at 295 nm as a function of temperature and obtained the T_m values. As shown in **Table 3** and **Fig. S3**, the melting curves of the G-rich DNA presented a standard inverted “S” type at 295 nm which is characteristic of a G-quadruplex structure in the presence/absence of **14a–c** and **16c**, indicating that the G-rich DNA could form a G4-DNA structure and the compounds may bind to such structure under experiment conditions. Furthermore, the ΔT_m values of compounds **14a–c** and **16c** increased in a concentration-dependent manner compared to the T_m (38.33 ± 0.07 °C) of the G-rich DNA alone. It was noteworthy that the ΔT_m values for **14c** are biggest relative to those for **14a**, **14b** and **16c** at each of used concentrations, of which the biggest ΔT_m value for **14c** at 8 μ M is 24.34 °C and the

smallest one for **14b** at 2 μM is 4.82 $^{\circ}\text{C}$, implying that **14c** could most strongly interact with and stabilize the telomeric G4-DNA's among all tested compounds.

Table 3.

T_m ($^{\circ}\text{C}$) values for Tel-26nt G-rich DNA in the presence/absence of 4,5-diazafluorene derivatives **14a-c** and **16c**.

Compound concentration	14a	14b	14c	16c
	T_m ($^{\circ}\text{C}$) ^a			
0 μM	38.33 \pm 0.07	38.33 \pm 0.07	38.33 \pm 0.07	38.33 \pm 0.07
2 μM	43.97 \pm 0.11	43.15 \pm 0.04	53.11 \pm 0.08	43.44 \pm 0.09
4 μM	45.57 \pm 0.09	43.96 \pm 0.06	56.08 \pm 0.05	44.91 \pm 0.12
8 μM	48.56 \pm 0.06	45.71 \pm 0.09	62.67 \pm 0.11	46.98 \pm 0.13

^aStandard deviation is given.

2.5 Specific interaction of 4,5-diazafluorene derivatives with telomeric G-quadruplexes

Circular dichroism (CD) spectroscopy is regarded as an important method to explore the DNA secondary structure, in particular G-quadruplex structure [48–50], but X-ray diffraction or NMR spectroscopy. To clearly clarify the specific binding of 4,5-diazafluorene derivatives to target DNA's at extracellular molecular level, we examined the interaction properties of both compounds **14c** and **16c** with 26nt telomeric DNA's (G-rich DNA and ds-DNA) and Mut-DNA (**Table 2**) by using the CD technique. The **14c** and **16c** are two representative compounds of 4,5-diazafluorene derivatives, the former exhibiting strongest inhibitory activity and best selectivity for A549 cells in CCK-8 assay (**Fig. 2, Table 1**) and strongest affinity to 26nt telomeric G-rich DNA in EMSA (**Fig. 3**) and UV-melting experiments (**Table 3**); the latter with a thioxothiazolidinone-oxadiazole moiety having weaker inhibitory activity against examined cancer cells (**Fig. 1**) and weakest affinity to 26nt telomeric G-rich DNA in EMSA (**Fig. 3**).

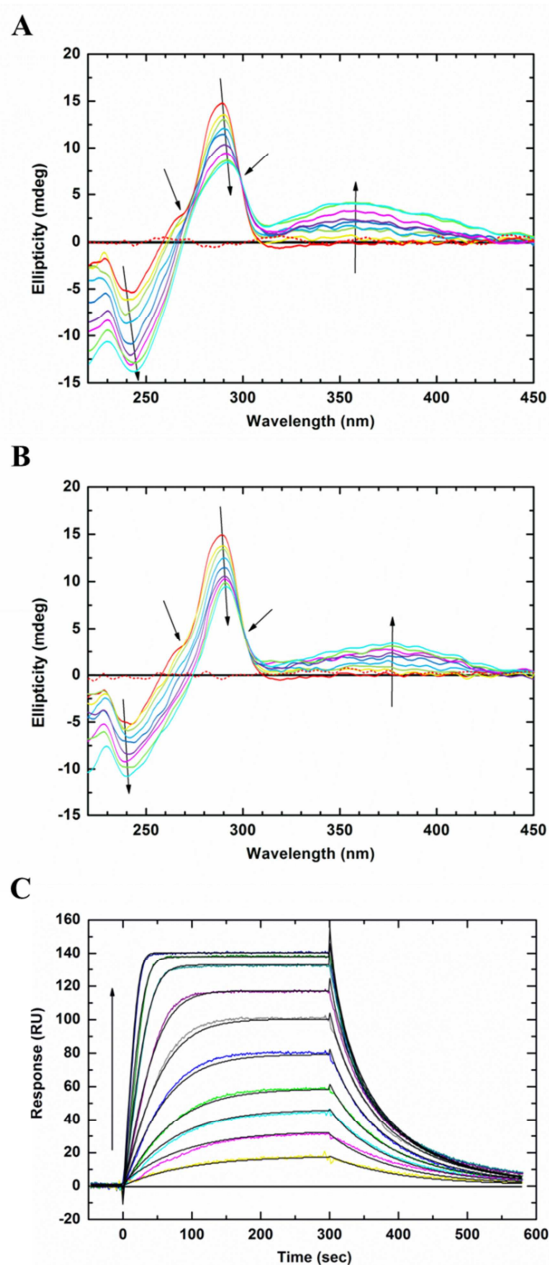


Fig. 4. The ability of 4,5-diazafluorene derivatives to specifically interact with G-quadruplex structures formed in a 26nt telomeric single stranded DNA sequence (G-rich DNA in **Table 2**) by CD (**A** and **B**) and SPR (**C**). Arrows at 240-245 nm (**A**) and 240-241 nm (**B**) denote the change of negative peak of telomeric G-quadruplex with the increase of the **14C** and **16C** concentration, respectively; an arrow at 270 nm (**A** and **B**) denotes the shoulder band of a 3+1 telomeric G-quadruplex structure; arrows at 290-292 nm (**A**) and 290-291.5 nm (**B**) denote the change of positive peak of telomeric G4-DNA with the increase of the **14C** and **16C** concentration, respectively; arrows near 298.5 nm (**A**) and 300.5 nm (**B**) denote the isoelliptic points; arrows at 358 nm (**A**) and 377 nm (**B**) denote the change of ICD positive band from 309-430 nm (**A**) and 311-435 nm (**B**) with the increase of the **14C** and **16C** concentration, respectively. CD spectra for 26nt telomeric G-rich DNA sequences of human chromosome in 10 mM K^+ by titration of the compounds at the ratio of a compound to DNA (r), 0.0, 0.25, 0.5, 1.0, 2.0, 3.0, 4.0, 5.0, 6.0 at concentrations of a compound ranging from 0.0 μ M (red curve, highest positive peak for DNA alone) to 24 μ M (cyan curve, lowest negative peak). All experiments were performed in a buffer (pH 7.4) containing 10 mM Tris-HCl, 10 mM KCl, 0.1 mM EDTA, and a sample of 4 μ M G-rich DNA (in single strand) dissolved in the buffer was incubated for 24 h after annealing at 95 $^{\circ}$ C. Red solid curve: DNA alone; red dotted line: compound alone. (**C**) A typical SPR

sensorgram for the interaction of the **14C** with the G-quadruplex structure formed in a G-rich DNA (Table 2) immobilized on the surface of a sensor chip SA. The binding response is changed with time. The data are globally fitted to a 1:1 interaction model with a mass transfer effect. Experimental curves are shown in color and fitting curves in black. The association phase was allowed to run for 300 sec to reach steady state and the dissociation phase for 280 sec for all concentrations used. Concentrations of the **14C** were used according to arrow direction: 6.25 (yellow), 12.5 (magenta), 25.0 (cyan), 50.0 (spring green), 100 (blue), 200 (gray), 400 (dark magenta), 600 (sky blue), 800 (sea green), and 1000 nM (dark blue, highest curve), respectively. Each experiment was carried out in triplicate.

Table 4.

Binding kinetic constants of **14c** to DNA's by SPR^a.

DNA	k_a [$M^{-1}s^{-1}$]	k_d [s^{-1}]	K_A [M^{-1}]
G-rich DNA	$6.68(\pm 0.12)^b \times 10^6$	$9.49(\pm 0.20) \times 10^{-2}$	$7.04(\pm 0.16) \times 10^7$
ds-DNA	$1.13(\pm 0.08) \times 10^3$	$2.58(\pm 0.10) \times 10^{-2}$	$4.38(\pm 0.13) \times 10^4$

^a k_a , association rate constant with a unit of $M^{-1}s^{-1}$; k_d , dissociation rate constant with a unit of s^{-1} ;

K_A , association equilibrium constant with a unit of M^{-1} ; $K_A = k_a/k_d$;

^b Standard deviation is given in parentheses.

As shown in **Fig. 4A**, and **B**, CD spectrum of the G-rich DNA alone (red solid line) presented a strong positive band at 290 nm, a shoulder band around 270 nm and a relatively shallow negative band at 240 nm, which is characteristic of a hybrid type of G4-DNA structure, also named a 3+1 G-quadruplex one [39,50,36], possibly including a small amount of other G-quadruplex ones [50,51], which is in good agreement with EMSA results in **Fig. 3**; whereas two compounds alone both are non-optically active, there existing not any CD bands (red dotted line). No too much red shift with a typical positive band near 290 nm and a negative band near 240 nm and the isoelliptic points at 358 nm and 377 nm were observed in the presence of **14c** and **16c**, respectively, indicating the two-state nature of the structural transition between the quadruplexes upon compound binding. More importantly, CD spectra of the G-rich DNA exhibited great difference in peak intensity and the feature of induced CD (ICD) in the presence of **14c** and **16c**, respectively. With gradual titration of **14c** or **16c** into the G-rich DNA at the ratios of compound/DNA, 0.25:1, 0.5:1, 1.0:1, 2.0:1, 3.0:1, 4.0:1, 5.0:1 and 6.0:1, the 290 nm positive peak intensity of the G4-DNA CD spectra progressively decreased up to saturation, and the 240 nm negative bands gradually became more negative up to a steady state, characteristic of a mixture of G4-DNA structures with an external loop(s) [38,52], with induced CD (ICD) spectra

ranging from 309 nm to 430 nm for **14c** or from 311 nm to 435 nm for **16c**; however, it was found that **14c** could cause bigger change in peak intensity and the feature of induced CD (ICD) than **16c**.

To investigate the binding selectivity of 4,5-diazafluorene derivatives to G4-DNA vs double-stranded DNA, we have measured CD spectra of the 26nt telomeric double-stranded DNA (ds-DNA, **Table 2**), in the presence and absence of representative **14c** or **16c**. As seen in **Fig. S4A** and **B**, the CD spectrum of the ds-DNA alone was characteristic of double-stranded DNA structure with strong positive and negative bands at 277 nm and at 241 nm, respectively [53]. With gradual titration of **14c** or **16c** into the ds-DNA at increasing concentrations of 4, 8, 16 μM , only less change in positive/negative peak intensity of ds-DNA and no ICD were observed and **14c** possessed slightly strong influence on ds-DNA than **16c**, which is in line with the results of T_m ($^{\circ}\text{C}$) values (**Table 3**), suggesting that this kind of compounds own stronger selectively binding to 26nt telomeric G4-DNA's over ds-DNA. Also, CD spectra of Mut-DNA (**Figs. S4C** and **D**) as a negative control was measured in the presence and absence of **14c** or **16c** under the same experimental conditions as above used ones, which cannot form any G-quadruplex structure due to the substitution of cytosine base for the middle guanine base of each of four three-Guanine-runs in G-rich DNA (**Table 2**). These data showed that Mut-DNA alone was typical of a freedom single-stranded DNA structure with a positive band at 281 nm and a negative band at 246.5 nm, and no influence was observed in the presence of compounds.

Collectively, this study suggests that the **14c** could gradually convert the 3+1 G-quadruplex structure formed in the G-rich DNA alone to a mixture of ones with an external loop(s), consistent with gel electrophoresis results shown in **Fig. 3**, and specifically bind to 26nt telomeric G4-DNA. Also, **16c** can result in less change of the CD spectra of 26nt telomeric DNA's.

To further evaluate the binding affinity, specificity and stoichiometry of 4,5-diazafluorene derivatives to target DNA's, we selected surface plasmon resonance (SPR) technique to have examined the interaction natures of a representative compound **14c** with G-rich DNA, Mut-DNA and ds-DNA (**Table 2**). SPR is a valuable and extensively used method for the study on the interaction between DNA's and small molecules [54–56], especially in recent years on G-quadruplexes [57,58] and telomerase inhibitors [59]. As shown in **Figs. 4C, S5** and **Table 4**, the quantitative SPR results provide strong evidence for a much greater binding affinity and

specificity of the **14c** to the 26nt human telomeric G4-DNA with an association equilibrium constant (K_A) of $7.04(\pm 0.16) \times 10^7 \text{ M}^{-1}$ than to the double-stranded DNA sequence (ds-DNA, **Table 2**) with a K_A of $4.38(\pm 0.13) \times 10^4 \text{ M}^{-1}$, indicating a more than 1000-fold increase in the binding affinity to G4-DNA relative to ds-DNA. We employed a 1:1 global theoretical fitting model with mass transport to experimental results. It was observed that experimental curves in color and fitting curves in black shown in **Fig. 4C** are quite well fitting and binding of the compound to the target DNA sequence at relatively higher concentrations of 800 to 1000 nM reached to saturation to obtain better steady states, implying a quite possible 1:1 stoichiometry of **14c** to the G4-DNA. In contrast, the **14c** was found to bind weakly to ds-DNA relative to G4-DNA (**Fig. S5** and **Table 4**), which is in accordance with results by CD (**Figs. 4A** and **S4A**) and T_m value analysis (**Table 3**). It is noticeable that almost no binding of the examined **14c** to Mut-DNA was observed at experimental concentrations, but there was large nonspecific binding at higher concentrations and hence precise interaction parameters between the **14c** and Mut-DNA were not obtained. In short, our studies suggest that the **14c** possesses quite strong binding and well selective abilities to G4-DNA over ds-DNA and Mut-DNA at the compound/G4-DNA ratio of 1:1. In addition, no 2:1 binding motif of **14c** to G4-DNA was found despite high concentrations being used.

2.6 *In-vitro* inhibition of telomerase activity by compounds **14a–c** and **16c**

Telomerase is highly expressed in a large proportion of human cancers relative to the very low level in normal somatic cells and its major function is to maintain the length of telomeric DNA by catalytically synthesizing telomeric DNA repeats. Because of such differential expression between human cancer and normal somatic cells, telomerase has been regarded as an anticancer target [60]. Thus, measurement of telomerase processivity/activity is very important to assess the inhibitory properties of small molecules against telomerase and commonly performed by the telomerase repeat amplification protocol (TRAP) assay [61]. As seen in **Fig. 5**, telomerase activity in the presence/absence of compounds **14a–c** in A549 cells was investigated by TRAP assay and differential ladders of telomeric DNA were observed at the increasing compound concentrations: 0, 2, 4, 8 μM . The result was found that the ability of **14a–c** to inhibit telomerase activity was in the order: **14c**>**14a**>**14b**, with strongest telomerase inhibition activity for **14c** being 61.66 % at 8 μM relative to that without **14c** (**Fig. 5B**). Furthermore, it was determined that

the **14c** can give rise to a good inhibitory effect on the telomerase activity of the positive control cells in the kit, as shown in **Fig. S6**. This result suggests that the 4,5-diazafluorene derivatives may directly or indirectly inhibit telomerase activity through their interaction with telomeric G4-DNA, leading to cancer cell apoptosis.

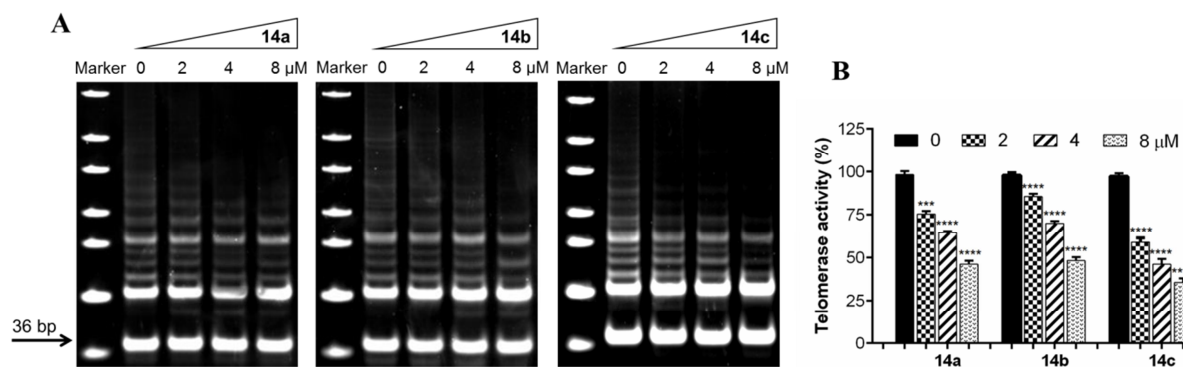


Fig. 5. Ability of telomerase activity inhibition by compounds **14a**, **14b** and **14c**. (A) Telomerase activity inhibition mediated by compounds at the increasing concentrations, 0, 2, 4 and 8 μM in A549 cells. The arrow presents a 36 bp internal control. (B) Telomerase activity was quantitated as the percent of the corresponding control. The mean of three independent experiments with comparable results was shown. Error bars indicate \pm SD.

2.7. Suppression of the examined cancer cell migration by compounds **14a–c**

It was reported that the telomerase activity was generally closely related to the metastasis and invasion of cancer cells [62,63]. In combination with the UV-melting assays and Trap assay, the compounds **14a–c** could strongly interact with and significantly stabilize telomeric G4-DNA structures and might inhibit telomerase activity, thereby do the metastasis and invasion of cancer cells. Therefore, we examined the effect of **14a–c** on the migration of A549, AGS, HepG2 and MCF-7 cells by *in-vitro* wound healing assay. As shown in **Fig. 6**, **Fig. S7** and **Table S1**, all of the compounds **14a–c** can obviously inhibit the migration of the tested cancer cells in a concentration-dependent manner and exhibited strongest migratory inhibitory effects on AGS cells amongst four cancer cells at each of 0.1, 0.2, 0.4 μM . It was worth noting that **14c** possessed strongest inhibitory ability to four cancer cells amongst three compounds, with the order of cell inhibitory ability being **14c**, **14a** and **14b**, but for A549 at 0.4 μM and for HepG2 at 0.2 and 0.4 μM , which is partly supportive of the above-mentioned experimental results. These results suggest that 4,5-diazafluorenes (**14a–c**) could effectively suppress the mobility of the four cancer cell lines at the low level of drug concentration.

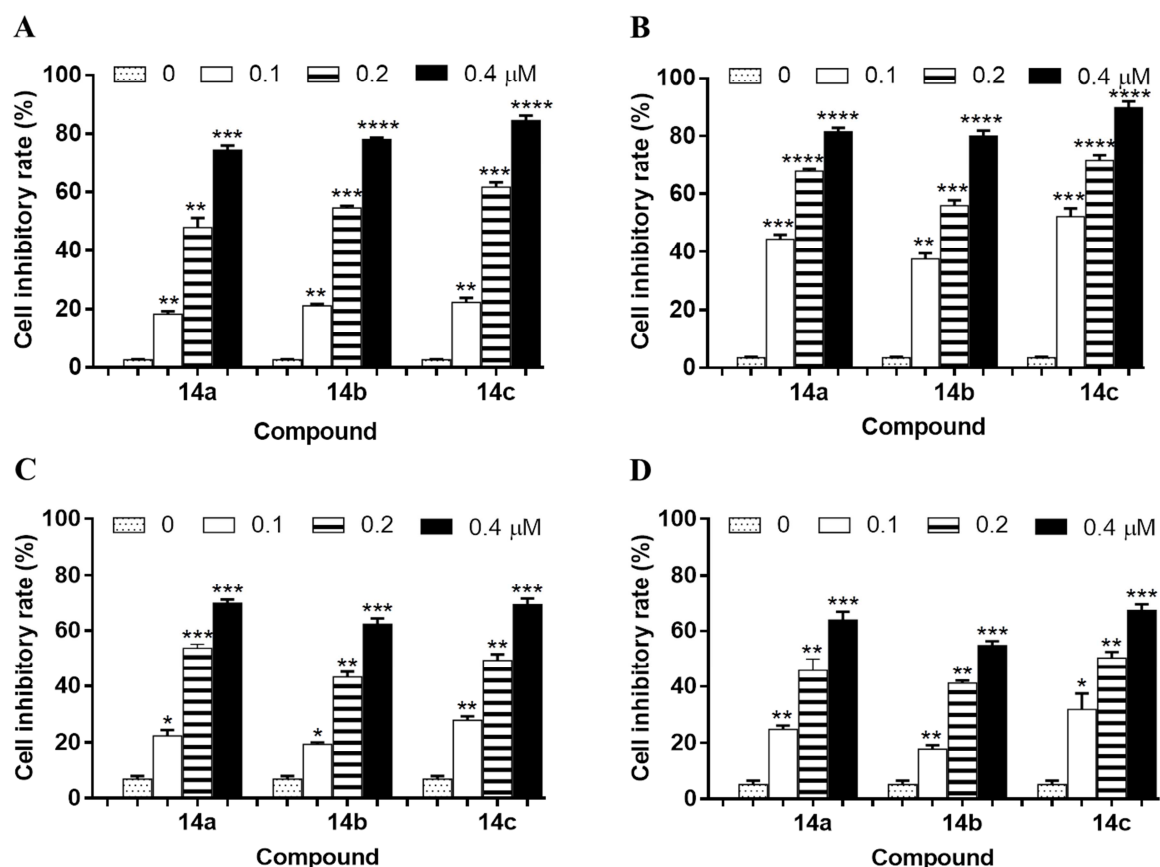


Fig. 6. Effect of compounds **14a-c** on the mobility of A549 (A), AGS (B), HepG2 (C) and MCF-7 (D) cell lines. The mobility changes of A549 cells in the presence and absence of **14a-c** at the concentration of 0, 0.1, 0.2, and 0.4 μM for 48 h, respectively. Cell inhibitory rate (%) for suppression of the migration in cancer cells as a function of concentrations of compounds **14a-c**. The % cell inhibitory rate was calculated by the equation: cell inhibitory rate (%) = $(1 - D_{\text{drug}}/D_{\text{control}}) \times 100\%$, where D_{drug} is mean distance of cell migration in drug group, D_{control} is mean distance of cell migration in control group; Values are the means \pm S.D. ($P < 0.05$).

2.8. Docking and UV-Visible spectral studies on the interaction of 4,5-diazafluorenes with telomeric G4-DNA

Such Structures of these small molecules with an extended planar aromatic system can facilitate compounds easily stacking on the G-quartet through π - π interactions [39,64], which are similar to a G-quartet in size and shape. Herein, LibDockin Discovery Studio 4.0 was utilized to investigate the interactions of compounds **14a-c** and **16c** with the target, telomeric G-quadruplex (PDB ID: 5MVB, a mode of a 3+1 typical telomeric G-quadruplex). As shown in **Figs. 7, S8** and **Table 5**, the results illustrated that the ligands **14a-c** and **16c** stack on the top capping of the 5' tetrad, surrounded by the DNA bases A3, G4, G12, T13, T14, A15, G16 and G22. The ranking of LibDock Score is consistent with the results obtained in the UV-melting, EMSA and CD studies.

The 4,5-diazafluorene skeleton, pyrazol, rhodanine, 1,3,4-oxadiazole and phenyl ring all could make intermolecular π - π interactions with DNA bases (magenta dash line). The dimethylaminopropyl side chain at N1-position of pyrazol moiety can well extend to the loop region at the 5' end. Additionally, the intermolecular hydrogen bonds could be found between the dimethylaminopropyl side chain and DNA bases A3, T13, T14 and A15 (green dash line in **Fig. S8**). Surprisingly, some intramolecular H-Bond interactions were found between the dimethylaminopropyl group and N14 in the pyrazol ring of compounds **14a-c**. It gives rise to more rigid conformations, which makes a good steric shape complementary between compounds **14a-c** and G-quadruplex (i.e. **14c** in **Fig. 7**). All these interactions and steric shape factor make significant contribution to the potency. The ring number of compounds **14a-c** is less than that of **16c**, and the receptor-ligand complex of the former shows less π - π interactions. The better potency of the former could be very likely due to the contribution of the N-substituent group in the pyrazol moiety. It might increase the potency if 1,3,4-oxadiazole group near the G-tetra center is replaced with a hydrophobic aromatic ring or other multiple rings with substituents. Taken together, the docking results indicate that **14a-c**, especially **14c**, can indeed quite fit to such G4-DNA structure and strongly bind to the target at the **14a**/G4-DNA ratio of 1:1 with a highest LibDock score of 193.929 among the examined compounds, which supports the result of the stoichiometry in SPR (**Fig. 4C**). These molecular docking data provide certain theoretical support for experimental results and the next optimization.

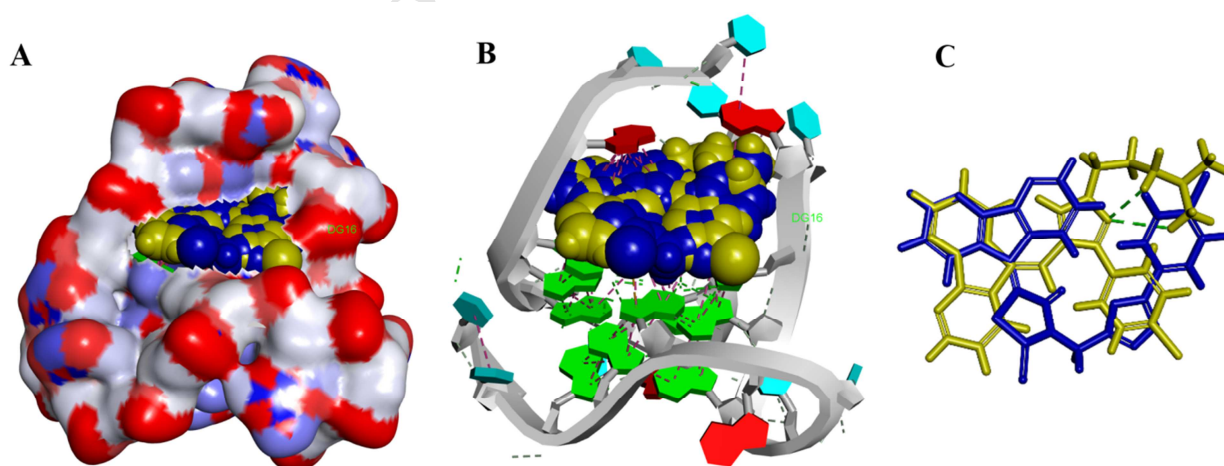


Fig. 7. Highly occupied binding modes of compounds **14c** and **16c** with 5MVB. 5MVB is represented by its soft atom charge surface in **A**, while its backbone model is shown in **B**. Compounds **14c** and **16c** extracted from the complex are shown in **C**. **14c** is shown in yellow CPK and stick models, and **16c** is shown in blue CPK and stick models. The compound **14c** has the highest Molecular_3D_SASA (the total solvent accessible surface area) of 695.86 \AA^2 , while compound **16c** has thirty less than that of the former.

Table 5.

The LibDock scores and docking interactions of compounds (**14a-c**, **16c**) with human telomeric DNA G-quadruplex (PDB ID: 5MVB).

Compound	LibDock score (k.cal/mol)	Interacting residues	Interacting atoms
14a	192.227	A3, G4, G12 A15, G16, G22	4,5-Diazafluorene - A3, G4, G12; Pyrazol - A3, G12, G16; Phenyl -G16, G22; Intramolecular H-bond - 14a:H48 - 14a:N14 Intermolecular H-bond - 14a:H43 - A:DA3:N1; 14a:H49 - A:DA15:N3; Hydrophobic - 14a:H51 - A:DA15 Halogen bond - A:DG16:N7 - 14a:F22.
14b	191.007	A3, G4, G12 T13, T14, G16, G22	4,5-Diazafluorene - A3, G4, G12; Pyrazol - A3, G12, G16; Phenyl - G16, G22; Intramolecular H-bond - 14b:H46 - 14b:N14; 14b:H51 - 14b:N14; 14b:H52 - 14b:N14; Intermolecular H-bond - 14b:H42 - A:DA3:N1; 14b:H46 - A:DT14:OP2; 14b:H47 - A:DT14:OP2; 14b:H48 - A:DT13:O3'; 14b:H49 - A:DT14:OP2; 14b:H42 - A:DA3:N1; 14b:H46 - A:DT14:OP2; Hydrophobic - A:DG16 - 14b:Cl22; A:DG22 - 14b:Cl22.
14c	193.929	A3, G4, G12 G16	4,5-Diazafluorene - A3, G4, G12; Pyrazol - A3, G12, G16; Phenyl - G16; Intramolecular H-bond - 14c:H47 - 14c:N14; 14c:H48 - 14c:N14; Intermolecular H-bond - 14c:H43 - A:DA3:N1; Hydrophobic - A:DG16 - 14c:Br22.
16c	189.045	A3, G4, G12 A15, G16, G22	4,5-Diazafluorene - A3, G4, G12; Rhodanine - G4, G22; 1,3,4-oxadiazole - G16, G22; Phenyl -A15, G16; Intermolecular H-bond - A:DT14:H5'2 - 16c:Br28; Hydrophobic - A:DA15 - 16c:Br28; Pi-Sulfur -16c:S11 - A:DG4; 16c:S29 - A:DG22.

To gain insight into the interaction mode of 4,5-diazafluorenes with the telomeric G4-DNA, we examined the UV-Vis spectral properties of a representative 4,5-diazafluorene compound, **14c**, gradually titrated with the 26nt telomeric G-rich DNA (G-rich DNA in **Table 2**). UV-Visible spectroscopy is an important and extensively applied technique for interpreting the interaction

mode of ligands with DNA. As seen in **Fig. S9**, the maximum absorption band of **14c** is located around 331.5 nm in the absence of G4-DNA. With the addition of G4-DNA, a striking spectral change was observed that a flat and broad absorption band containing a dominant peak and a shoulder one near 366.5 nm and 331.5 nm, respectively, occurred, the solet band exhibited more hyperchromicity and bathochromically shifted from 331.5 nm to 366.5 nm at the increasing DNA concentrations ranging from 0 to 40 μ M, suggesting that the interaction of **14c** with G4-DNA takes places through external binding/stacking [65]. At the same time, another important fact is that the isobestic point was not a sharp, tight single point, indicating that the interaction involves multiple steps [65]. More importantly, when such interaction reached saturation, i.e. no change in maximum absorption intensity and absorption wavelength with increasing compound concentration, the 1:1 stoichiometry of the interaction of **14c** with G4-DNA can be inferred (the inset in **Fig. S9**). The UV-Visible data are in good agreement with results obtained by molecular docking and SPR assays.

3. Discussion

The antiproliferative activities of all the synthesized 4,5-diazafluorene derivatives were evaluated against A549, AGS, HepG2 and MCF-7 cells and MRC-5 cells as a control by CCK-8 assay and the results disclosed following some structure-activity relationships. SAR studies revealed that various substitutions on the phenylpyrazole moiety had significant influence on bioactivity. The R_1 group of pyrazole ring plays a vital role in antiproliferative activity. Hydrogen and aromatic substituents at the N-1 nitrogenation on the pyrazole ring like benzyl and 2,4-dinitrophenyl groups did not influence on bioactivity. Compounds **11a–13d** with such groups exhibited moderate activity; while an aliphatic substituent, N,N^1 -dimethylaminopropyl group, noticeably influences the bioactivity of examined compounds, leading to the findings that the **14a–c** with such a group showed more excellent anti proliferative activity than the **11a–13d**. Another notable fact is that the effect of para substituents on the benzene ring on the bioactivity of examined compounds was found in the following order: bromo, fluoro, chloro and methyl, therefore, the **14c** almost exhibited best activity and strongest affinity to the target in all finished experiments amongst examined compounds. However, introduction of the thioxothiazolidinone ring and the phenyloxadiazole moiety to 4,5-diazafluorene mother structure cannot obviously

increase the bioactivity of compounds **15**, **16a–c** compared with **11a–13d**, **14a–c**. All in all, based on the SAR study we conclude that modifications on 4,5-diazafluorene-pyrazole contribute to the effort for finding new promising anticancer drugs.

In addition, in recent two decades, increasing evidence has shown that a large number of small molecules possess the ability to inhibit telomerase and hence do antitumor activity. In particular, small molecules that induce the telomeric guanine-rich single-stranded DNA to form and stabilize G-quadruplex structures can block the function of telomerase, such as porphyrins, acridines, and the natural product telomestatin [66–73]. Telomerase as a drug target is over expressed in mostly cancer cells and it is closely associated the metastasis, invasion and apoptosis of some cancer cells. Hence, we initially explored whether such resultant antitumor activity was obtained by the interaction of the novel 4,5-diazafluorene derivatives with telomeric G4-DNA which inhibits telomerase activity. Experimental results at extra/intracellular level are especially inspiring that **14a–c** derivatives had stabilizing ability towards human telomere G-quadruplex DNA, in particular **14c**, which are consistent with those by molecular docking studies, and mediated the inhibition of telomerase activity. Furthermore, docking studies indicate that the 1-*N,N*¹-dimethylaminopropyl and 3-(4-bromophenyl) substituents on **14c** have advantage over others, when binding to G4-NDA. These data also imply that the introduction of 3-(3-(4-bromophenyl)-1H-pyrazol-1-yl)-*N,N*-dimethylpropan-1-amine substituent on 4,5-diazafluorene was successful.

4. Conclusion

In summary, 4,5-diazafluorene derivatives bearing phenylpyrazole and thioxo thiazolidinone/thioxothiazolidinone-phenyloxadiazole moieties were designed, synthesized and their antiproliferative activity evaluated against A549, AGS, HepG2 and MCF-7 cell lines, and also their interaction mechanism with telomeric G4-DNA preliminarily explored. The compounds **14a–c** with a phenylpyrazole group showed stronger inhibitory activities with IC₅₀ values in the range of 1.13–11.77 μM. In particular, the compound **14c** is the most efficient antiproliferative agent amongst the examined compounds including cisplatin as a positive control against A549 (IC₅₀ = 1.13 μM), AGS (IC₅₀ = 1.81 μM) and MCF-7 (IC₅₀ = 5.27 μM) cells, but HepG2 cells (IC₅₀ = 3.4 μM). Likewise, the results by wound healing assay also are in agreement with the

above results, showing that the inhibitory effects of **14a–c** on the mobility of four cancer cells are outstanding. 4,5-diazafluorenes bearing a phenylpyrazole group could effectively inhibit invasion and metastasis of cancer cells and the **14c** possesses strongest migration inhibitory ability, but for HepG2 cells at 0.2 and 0.4 μM . Furthermore, based on EMSA, UV-melting, CD, SPR, UV-Vis spectral assay, molecular docking study and TRAP assay results, **14a–c**, especially **14c**, can strongly interact with 26nt telomeric G-quadruplexes and mediate telomerase activity decrease, consequently causing the inhibition of cell proliferation. Our study demonstrate that 4,5-diazafluorene derivatives with a phenylpyrazole group as a novel class of G4-DNA mediated telomerase inhibitors may be developed as potential anticancer agents.

5. Experimental protocols

5.1. General

All solvents and chemicals were analytic pure, obtained from commercial suppliers and used without further purification unless otherwise stated. A Millipore MilliQ water purification system produced 18 M Ω water used to prepare buffer solutions. The melting points of analogues were observed on the melting point detector (XT-5A). Reaction processes were monitored by TLC on silica gel-precoated F254 Merck plates and the thin layer plates were examined under the UV lamps (254 nm and 365 nm). $^1\text{H-NMR}$ spectra were recorded in pure $\text{CDCl}_3/\text{DMSO-}d_6$ on Bruker NMR spectrometers (AVANCE-III 500 MHz) using tetramethylsilane (TMS) as internal standard. Chemical shifts were expressed in δ , ppm. Mass spectra were measured on an Agilent 6210 TOF LC/MS (USA). Purity of compounds was analyzed by HPLC on a Shimadzu LC-20AT instrument. DNA oligomers/primers were purchased from Sangon (Shanghai, China), and used without further purification. These oligomers were purified by HPLC, identified by HPLC-CE and TOF Mass, and exhibited single-band electrophoretic mobilities in denaturing polyacrylamide gel electrophoresis with stated purities of $\geq 95\%$. The sequences of (biotin-modified) DNA oligomers used are listed in **Table 2**. Solutions of the DNA oligomers were prepared as follows: an oligonucleotide sample dissolved in a specified used buffer was heated at 95 $^\circ\text{C}$ for 5 min and allowed to slowly cool to room temperature at 1 $^\circ\text{C}/1$ min over a period of several hours and then incubated at 4 $^\circ\text{C}$ overnight. All cell lines were supplied by the Type Culture Collection of the Chinese Academy of Sciences, Shanghai, China. Sensor chip SA were

purchased from BIAcore AB (Sweden). All other commercially available reagents and solvents were purchased and used without further purification unless otherwise stated. MilliQ water was used to prepare buffer solutions.

5.1.1. General procedure for the synthesis of target compounds **11–14**.

A mixture of 4,5-diazafluorene **6** (1.0 mmol), ammonium acetate (4.0 mmol), and 1.1 mmol **7a–d**, **8a–d**, **9a–d**, **10a–c** respectively, in glacial acetic acid (20 mL) was heated at 110 °C with stirring for 6 h. The reaction was monitored by TLC for completion. The resultant solution was concentrated and neutralized with 20% aqueous ammonia. The white and yellow precipitate was collected, washed with water and purified by silica gel chromatography (dichloromethane/methanol, 15:1) to afford pure white products (**11a–d**, **12a–d**, and **14a–c**) and yellow crystals (**13a–d**), respectively. The yield, melting point, purity and spectral data of each compound are given as follows.

5.1.1.1. 5-((3-(4-Fluorophenyl)-1H-pyrazol-4-yl)methylene)-5H-cyclopenta[2,1-b:3,4-b']dipyridine (**11a**)

Pale yellow solid; yield: 85%; m.p.: 217–219 °C; purity by HPLC: 98.1%. ¹H NMR (DMSO-*d*₆, 500 MHz, ppm): δ 13.49 (br. s, 1H, N-H), 8.67 (dd, *J* = 5.0, 1.5 Hz, 1H, pyridine-H₈), 8.63 (dd, *J* = 5.0, 1.5 Hz, 1H, pyridine-H₂), 8.48 (dd, *J* = 8.0, 1.5 Hz, 1H, pyrazol-H₁₁), 8.22 (d, *J* = 7.5 Hz, 1H, pyridine-H₆), 7.89 (br. s, 1H, C-H₁₀), 7.72 (dd, *J* = 5.0, 1.5 Hz, 2H, benzene-H), 7.46 (dd, *J* = 5.0, 1.5 Hz, 1H, pyridine-H₄), 7.34 (dd, *J* = 5.0, 1.5 Hz, 1H, benzene-H), 7.32–7.29 (m, 3H, pyridine-H_{3,7} and benzene-H). MS (ESI) calcd for C₂₁H₁₃FN₄: 340.11, found: 341.1 (M+H⁺).

5.1.1.2. 5-((3-(4-Chlorophenyl)-1H-pyrazol-4-yl)methylene)-5H-cyclopenta[2,1-b:3,4-b']dipyridine (**11b**)

Pale yellow solid; yield: 83%; m.p.: 242–244 °C; purity by HPLC: 97.8%. ¹H NMR (DMSO-*d*₆, 500 MHz, ppm): δ 13.57 (br. s, 1H, N-H), 8.68 (d, *J* = 4.0 Hz, 1H, pyridine-H₈), 8.64 (d, *J* = 4.0 Hz, 1H, pyridine-H₂), 8.50 (d, *J* = 7.5 Hz, 1H, pyrazol-H₁₁), 8.21 (d, *J* = 6.5 Hz, 1H, pyridine-H₆), 7.90 (br. s, 1H, C-H₁₀), 7.71 (d, *J* = 7.5 Hz, 2H, benzene-H), 7.52 (br. s, 3H, pyridine-H₄ and benzene-H), 7.46 (dd, *J* = 7.5, 5.0 Hz, 1H, pyridine-H₇), 7.34 (dd, *J* = 7.5, 5.0 Hz, 1H, pyridine-H₃). MS (ESI) calcd for C₂₁H₁₃ClN₄: 356.08, found: 357.1 (M+H⁺).

5.1.1.3. *5-((3-(4-Bromophenyl)-1H-pyrazol-4-yl)methylene)-5H-cyclopenta[2,1-b:3,4-b']dipyridine (11c)*

Pale yellow solid; yield: 88%; m.p.:251–253 °C; purity by HPLC: 98.5%. ¹H NMR (DMSO-*d*₆, 500 MHz, ppm): δ 13.55 (br. s, 1H, N-H), 8.67 (dd, *J* = 4.5, 1.0 Hz, 1H, pyridine-H₈), 8.64 (dd, *J* = 5.0, 1.5 Hz, 1H, pyridine-H₂), 8.48 (dd, *J* = 7.5, 1.0 Hz, 1H, pyrazol-H₁₁), 8.21 (d, *J* = 7.0 Hz, 1H, pyridine-H₆), 7.89 (br. s, 1H, C-H₁₀), 7.65-7.53 (m, 5H, pyridine-H₄ and benzene-H), 7.46 (dd, *J* = 8.0, 5.0 Hz, 1H, pyridine-H₇), 7.34 (dd, *J* = 8.0, 5.0 Hz, 1H, pyridine-H₃). MS (ESI) calcd for C₂₁H₁₃BrN₄: 400.03, found: 401.0 (M+H⁺).

5.1.1.4. *5-((3-(P-tolyl)-1H-pyrazol-4-yl)methylene)-5H-cyclopenta[2,1-b:3,4-b']dipyridine (11d)*

Yellow solid; yield: 81%; m.p.:178–180 °C; purity by HPLC: 98.3%. ¹H NMR (DMSO-*d*₆, 500 MHz, ppm): δ 13.46 (br. s, 1H, N-H), 8.67 (dd, *J* = 4.5, 1.0 Hz, 1H, pyridine-H₈), 8.64 (dd, *J* = 4.5, 1.0 Hz, 1H, pyridine-H₂), 8.45 (dd, *J* = 7.5, 1.5 Hz, 1H, pyrazol-H₁₁), 8.28 (d, *J* = 7.0 Hz, 2H, benzene-H), 7.86 (br. s, 1H, C-H₁₀), 7.58 (d, *J* = 8.0 Hz, 2H, pyridine-H_{4,6}), 7.45 (dd, *J* = 8.0, 5.0 Hz, 1H, benzene-H), 7.36 (dd, *J* = 8.0, 5.0 Hz, 1H, benzene-H), 7.28 (br. s, 2H, pyridine-H_{3,7}), 2.33 (s, 3H, CH₃). MS (ESI) calcd for C₂₂H₁₆N₄: 336.14, found: 337.2 (M+H⁺).

5.1.1.5. *5-((1-Benzyl-3-(4-fluorophenyl)-1H-pyrazol-4-yl)methylene)-5H-cyclopenta[2,1-b:3,4-b']dipyridine (12a)*

White solid; yield: 74%; m.p.:232–234 °C; purity by HPLC: 98.6%. ¹H NMR (CDCl₃, 500 MHz, ppm): δ 8.70 (dd, *J* = 4.5, 1.0 Hz, 1H, pyridine-H₈), 8.63 (dd, *J* = 4.5, 1.0 Hz, 1H, pyridine-H₂), 8.05-8.01 (m, 2H, benzene-H), 7.74 (s, 1H, pyrazol-H₁₁), 7.72-7.69 (m, 2H, pyridine-H_{4,6}), 7.45 (s, 1H, C-H₁₀), 7.44-7.36 (m, 5H, benzene-H), 7.30 (dd, *J* = 7.5, 4.5 Hz, 1H, benzene-H), 7.12-7.07 (m, 2H, pyridine-H_{3,7}), 7.04 (dd, *J* = 8.0, 4.5 Hz, 1H, benzene-H), 5.44 (s, 2H, CH₂). MS (ESI) calcd for C₂₈H₁₉FN₄: 430.16, found: 431.2 (M+H⁺).

5.1.1.6. *5-((1-Benzyl-3-(4-chlorophenyl)-1H-pyrazol-4-yl)methylene)-5H-cyclopenta[2,1-b:3,4-b']dipyridine (12b)*

White solid; yield: 77%; m.p.:260–262 °C; purity by HPLC: 98.7%. ¹H NMR (CDCl₃, 500 MHz,

ppm): δ 8.70 (dd, $J = 4.5, 1.0$ Hz, 1H, pyridine-H₈), 8.63 (dd, $J = 5.0, 1.5$ Hz, 1H, pyridine-H₂), 8.03-8.01 (m, 2H, benzene-H), 7.73 (s, 1H, pyrazol-H₁₁), 7.68-7.66 (m, 2H, pyridine-H_{4,6}), 7.45 (s, 1H, C-H₁₀), 7.44-7.41 (m, 2H, benzene-H), 7.40-7.36 (m, 5H, benzene-H), 7.31 (q, 1H, pyridine-H₇), 7.04 (q, 1H, pyridine-H₃), 5.44 (s, 2H, CH₂). MS (ESI) calcd for C₂₈H₁₉ClN₄: 446.13, found: 447.1 (M+H⁺).

5.1.1.7. 5-((1-Benzyl-3-(4-bromophenyl)-1H-pyrazol-4-yl)methylene)-5H-cyclopenta[2,1-b:3,4-b']dipyridine (**12c**)

White solid; yield: 78%; m.p.:263–265 °C; purity by HPLC: 98.3%. ¹H NMR (CDCl₃, 500 MHz, ppm): δ 8.70 (dd, $J = 5.0, 1.5$ Hz, 1H, pyridine-H₈), 8.62 (dd, $J = 5.0, 1.5$ Hz, 1H, pyridine-H₂), 8.02-8.00 (m, 2H, benzene-H), 7.73 (s, 1H, pyrazol-H₁₁), 7.62-7.59 (m, 2H, pyridine-H_{4,6}), 7.54-7.51 (m, 2H, benzene-H), 7.44 (s, 1H, C-H₁₀), 7.43-7.36 (m, 5H, benzene-H), 7.30 (q, 1H, pyridine-H₇), 7.04 (q, 1H, pyridine-H₃), 5.44 (s, 2H, CH₂). MS (ESI) calcd for C₂₈H₁₉BrN₄: 490.08, found: 491.1 (M+H⁺).

5.1.1.8. 5-((1-Benzyl-3-(p-tolyl)-1H-pyrazol-4-yl)methylene)-5H-cyclopenta[2,1-b:3,4-b']dipyridine (**12d**)

White solid; yield: 75%; m.p.:231–233 °C; purity by HPLC: 97.8%. ¹H NMR (CDCl₃, 500 MHz, ppm): δ 8.70 (dd, $J = 4.0, 1.0$ Hz, 1H, pyridine-H₈), 8.63 (dd, $J=4.5, 1.0$ Hz, 1H, pyridine-H₂), 8.10 (dd, $J = 8.0, 1.5$ Hz, 1H, benzene-H), 8.03 (dd, $J = 8.0, 1.5$ Hz, 1H, benzene-H), 7.74 (s, 1H, pyrazol-H₁₁), 7.62-7.61 (m, 2H, pyridine-H_{4,6}), 7.51 (s, 1H, C-H₁₀), 7.43-7.40 (m, 2H, benzene-H), 7.39-7.36 (m, 3H, benzene-H), 7.31 (q, 1H, pyridine-H₇), 7.23 (d, $J = 7.5$ Hz, 2H, benzene-H), 7.05 (q, 1H, pyridine-H₃), 5.45 (s, 2H, CH₂), 2.38 (s, 3H, CH₃). MS (ESI) calcd for C₂₉H₂₂N₄: 426.18, found: 427.2 (M+H⁺).

5.1.1.9. 5-((1-(2,4-Dinitrophenyl)-3-(4-fluorophenyl)-1H-pyrazol-4-yl)methylene)-5H-cyclopenta[2,1-b:3,4-b']dipyridine (**13a**)

Yellow solid; yield: 85%; m.p.:>310°C; purity by HPLC: 98.5%. ¹H NMR (DMSO-*d*₆, 500 MHz, ppm): δ 9.11 (s, 1H, benzene-H₁₇), 8.95 (d, $J = 1.0$ Hz, 1H, benzene-H), 8.71-8.70 (m, 2H, pyridine-H_{2,8}), 8.66 (d, $J = 4.5$ Hz, 1H, benzene-H), 8.56 (d, $J = 7.5$ Hz, 1H, pyrazol-H₁₁), 8.31

(d, $J = 9.0$ Hz, 1H, pyridine-H₆), 8.25 (d, $J = 8.0$ Hz, 1H, pyridine-H₄), 7.95 (s, 1H, C-H₁₀), 7.74-7.71 (m, 2H, benzene-H), 7.52-7.50 (m, 1H, benzene-H), 7.36-7.30 (m, 3H, benzene-H and pyridine-H_{3,7}). MS (ESI) calcd for C₂₇H₁₅FN₆O₄: 506.11, found: 507.1 (M+H⁺).

5.1.1.10. *5-((3-(4-Chlorophenyl)-1-(2,4-dinitrophenyl)-1H-pyrazol-4-yl)methylene)-5H-cyclopenta[2,1-b:3,4-b']dipyridine (13b)*

Yellow solid; yield: 85%; m.p.: >310 °C; purity by HPLC: 98.4%. ¹H NMR (DMSO-*d*₆, 500 MHz, ppm): δ 9.12 (s, 1H, benzene-H), 8.96 (br. s, 1H, benzene-H₁₆), 8.71 (d, $J = 5.5$ Hz, 2H, pyridine-H_{2,8}), 8.66 (d, $J = 4.0$ Hz, 1H, benzene-H), 8.56 (d, $J = 7.5$ Hz, 1H, pyrazol-H₁₁), 8.31 (d, $J = 9.0$ Hz, 1H, pyridine-H₆), 8.25 (d, $J = 7.5$ Hz, 1H, pyridine-H₄), 7.95 (s, 1H, C-H₁₀), 7.71 (d, $J = 8.5$ Hz, 2H, benzene-H), 7.56 (d, $J = 8.0$ Hz, 2H, benzene-H), 7.53-7.50 (m, 1H, pyridine-H₇) 7.36-7.34 (m, 1H, pyridine-H₃). MS (ESI) calcd for C₂₇H₁₅ClN₆O₄: 522.08, found: 523.1 (M+H⁺).

5.1.1.11. *5-((3-(4-Bromophenyl)-1-(2,4-dinitrophenyl)-1H-pyrazol-4-yl)methylene)-5H-cyclopenta[2,1-b:3,4-b']dipyridine (13c)*

Yellow solid; yield: 83%; m.p.: >310 °C; purity by HPLC: 98.6%. ¹H NMR (DMSO-*d*₆, 500 MHz, ppm): δ 9.12 (s, 1H, benzene-H₁₇), 8.96 (d, $J = 2.5$ Hz, 1H, benzene-H), 8.72-8.69 (m, 2H, pyridine-H_{2,8}), 8.65 (dd, $J = 6.0, 1.0$ Hz, 1H, benzene-H), 8.54 (dd, $J = 6.0, 1.0$ Hz, 1H, pyrazol-H₁₁), 8.30 (d, $J = 9.0$ Hz, 1H, pyridine-H₆), 8.24 (dd, $J = 8.0, 1.0$ Hz, 1H, pyridine-H₄), 7.94 (s, 1H, C-H₁₀), 7.68 (dd, $J = 7.0, 2.0$ Hz, 2H, benzene-H), 7.62 (dd, $J = 7.0, 2.0$ Hz, 2H, benzene-H), 7.50 (dd, $J = 8.0, 5.0$ Hz, 1H, pyridine-H₇), 7.35 (dd, $J = 8.0, 4.0$ Hz, 1H, pyridine-H₃). MS (ESI) calcd for C₂₇H₁₅BrN₆O₄: 566.03, found: 567.0 (M+H⁺).

5.1.1.12. *5-((1-(2,4-Dinitrophenyl)-3-(*p*-tolyl)-1H-pyrazol-4-yl)methylene)-5H-cyclopenta[2,1-b:3,4-b']dipyridine (13d)*

Yellow solid; yield: 82%; m.p.: >310 °C; purity by HPLC: 98.2%. ¹H NMR (DMSO-*d*₆, 500 MHz, ppm): δ 9.09 (s, 1H, benzene-H₁₇), 8.94 (d, $J = 2.5$ Hz, 1H, benzene-H), 8.71-8.68 (m, 2H, pyridine-H_{2,8}), 8.66 (d, $J = 4.5$ Hz, 1H, benzene-H), 8.54 (d, $J = 7.5$ Hz, 1H, pyrazol-H₁₁), 8.30-8.26 (m, 2H, pyridine-H_{4,6}), 7.93 (s, 1H, C-H₁₀), 7.58 (d, $J = 8.0$ Hz, 2H, benzene-H), 7.50 (dd, J

= 8.0, 5.0 Hz, 1H, pyridine-H₇), 7.35 (dd, $J = 8.0, 5.0$ Hz, 1H, pyridine-H₃), 7.28 (d, $J = 8.0$ Hz, 2H, benzene-H), 2.32 (s, 3H, CH₃). MS (ESI) calcd for C₂₈H₁₈N₆O₄: 502.14, found: 503.19 (M+H⁺).

5.1.1.13. 3-(4-((5H-cyclopenta[2,1-b:3,4-b']dipyridin-5-ylidene)methyl)-3-(4-fluorophenyl)-1H-pyrazol-1-yl)-N,N-dimethylpropan-1-amine (**14a**)

Pale yellow solid; yield: 78%, m.p.:208–210 °C; purity by HPLC: 98.7%. ¹H NMR (DMSO-*d*₆, 500 MHz, ppm): δ 8.67 (dd, $J = 5.0, 1.0$ Hz, 1H, pyridine-H₈), 8.64 (dd, $J = 5.0, 1.0$ Hz, 1H, pyridine-H₂), 8.47 (dd, $J = 8.0, 1.5$ Hz, 1H, pyridine-H₆), 8.34 (s, 1H, pyrazol-H₁₁), 8.26 (dd, $J = 8.0, 1.5$ Hz, 1H, pyridine-H₄), 7.86 (s, 1H, C-H₁₀), 7.73-7.70 (m, 2H, benzene-H), 7.46 (dd, $J = 8.0, 5.0$ Hz, 1H, pyridine-H₇), 7.32 (dd, $J = 8.0, 5.0$ Hz, 1H, pyridine-H₃), 7.27-7.24 (m, 2H, benzene-H), 4.29 (t, $J = 6.75$ Hz, 2H, CH₂), 2.33 (t, $J = 5.5$ Hz, 2H, CH₂), 2.20 (s, 6H, CH₃), 2.08-2.03 (m, 2H, CH₂). ¹³C NMR (CDCl₃ + CD₃OD-*d*₄, 126 MHz, ppm): δ 163.95, 161.98, 157.45, 155.52, 151.05, 149.86, 134.16, 131.78, 131.51, 131.04, 129.81, 129.66, 128.84, 127.75, 123.17, 122.77, 122.26, 115.89, 114.02, 55.86, 50.15, 44.44, 27.12. MS (ESI) calcd for C₂₆H₂₄FN₅: 425.2016, found: 426.2083 (M+H⁺), 448.1902 (M+Na⁺).

5.1.1.14. 3-(4-((5H-cyclopenta[2,1-b:3,4-b']dipyridin-5-ylidene)methyl)-3-(4-chlorophenyl)-1H-pyrazol-1-yl)-N,N-dimethylpropan-1-amine (**14b**)

Pale yellow solid; yield: 74%; m.p.:230–232 °C; purity by HPLC: 99.3%. ¹H NMR (DMSO-*d*₆, 500 MHz, ppm): δ 8.68 (d, $J = 4.5$ Hz, 1H, pyridine-H₈), 8.65 (d, $J = 4.5$ Hz, 1H, pyridine-H₂), 8.49 (d, $J = 7.5$ Hz, 1H, pyridine-H₆), 8.35 (s, 1H, pyrazol-H₁₁), 8.24 (d, $J = 8.0$ Hz, 1H, pyridine-H₄), 7.87 (s, 1H, C-H₁₀), 7.70 (d, $J = 8.5$ Hz, 2H, benzene-H), 7.49 (d, $J = 8.5$ Hz, 2H, benzene-H), 7.47-7.46 (m, 1H, pyridine-H₇), 7.35-7.32 (m, 1H, pyridine-H₃), 4.29 (t, $J = 7.0$ Hz, 2H, CH₂), 2.30 (t, $J = 6.5$ Hz, 2H, CH₂), 2.18 (s, 6H, CH₃), 2.08-2.02 (m, 2H, CH₂). ¹³C NMR (CDCl₃ + CD₃OD-*d*₄, 126 MHz, ppm): δ 156.33, 154.37, 149.54, 148.76, 148.69, 133.34, 133.14, 130.72, 130.53, 130.20, 130.01, 128.61, 128.25, 127.93, 126.83, 122.21, 121.72, 121.39, 113.00, 55.24, 49.52, 44.21, 26.99. MS (ESI) calcd for C₂₆H₂₄ClN₅: 441.1720, found: 442.1790 (M+H⁺), 464.1611 (M+Na⁺).

5.1.1.15. 3-(4-((5*H*-cyclopenta[2,1-*b*:3,4-*b'*]dipyridin-5-ylidene)methyl)-3-(4-bromophenyl)-1*H*-pyrazol-1-yl)-*N,N*-dimethylpropan-1-amine (**14c**)

Pale yellow solid; yield: 80%; m.p.:209–211 °C; purity by HPLC: 98.6%. ¹H NMR (DMSO-*d*₆, 500 MHz, ppm): δ 8.67 (dd, *J* = 5.0, 1.0 Hz, 1H, pyridine-H₈), 8.66 (d, *J* = 4.0 Hz, 1H, pyridine-H₂), 8.49 (dd, *J* = 8.0, 1.0 Hz, 1H, pyridine-H₆), 8.39 (s, 1H, pyrazol-H₁₁), 8.27 (dd, *J* = 8.0, 1.0 Hz, 1H, pyridine-H₄), 7.84 (s, 1H, C-H₁₀), 7.64 (br. s, 4H, benzene-H), 7.48-7.46 (m, 1H, pyridine-H₇), 7.36-7.33 (m, 1H, pyridine-H₃), 4.35 (t, *J* = 6.75 Hz, 2H, CH₂), 2.91 (t, *J* = 6.5 Hz, 2H, CH₂), 2.63 (s, 6H, CH₃), 2.24-2.21 (m, 2H, CH₂). ¹³C NMR (CDCl₃ + CD₃OD-*d*₄, 126 MHz, ppm): δ 156.23, 154.28, 149.72, 148.69, 148.64, 133.23, 130.93, 130.87, 130.59, 130.58, 130.18, 128.70, 128.55, 126.98, 122.31, 121.84, 121.68, 121.35, 113.13, 54.83, 49.30, 43.42, 26.25. MS (ESI) calcd for C₂₆H₂₄BrN₅: 485.1215, found: 486.1278 (M+H⁺), 508.1081 (M+Na⁺).

5.1.2. General synthetic procedure for the target compounds **15** and **16a–c**.

A mixture of 4,5-Diazafluoren-9-one **5** (1.0 mmol), ammonium acetate (4.0 mmol), and 1.1 mmol 2-(4-oxo-2-thioxothiazolidin-3-yl)acetic acid in glacial acetic acid (20 mL) was heated at 110 °C with stirring for 6 h. The reaction was monitored by TLC for completion. The resultant solution was concentrated and adjusted pH value to 6 with 20% aqueous ammonia. The yellow precipitate was collected, washed with water and purified by silica gel chromatography (dichloromethane/methanol, 20:1) to afford pure yellow product **15**. A solution of compound **15** (1.0 mmol) in 10.0 mL phosphorus oxychloride was added 4-substituted benzohydrazides (0.14 g, 1.0 mmol), and the reaction mixture was stirred at 105 °C for 5h, respectively, until the completion of the reaction checked by thin-layer chromatography (TLC). The resulting reaction mixture was poured into 100 mL ice water and adjusted pH value to 7 with sodium carbonate solution, extracted with dichloromethane (3×100 mL), dried with Na₂SO₄, filtered, concentrated and finally purified by silica gel chromatography (dichloromethane/methanol, 30:1) to afford pure yellow crystals **16a–c**. The yield, melting point and spectral data of each compound are given below.

5.1.2.1. 2-(5-((5*H*-cyclopenta[2,1-*b*:3,4-*b'*]dipyridin-5-ylidene)-4-oxo-2-thioxothiazolidin-3-yl)acetic acid (**15**)

Yellow solid; yield: 89%; m.p.: >310 °C; purity by HPLC: 97.7%. ¹H NMR (DMSO-*d*₆, 500 MHz, ppm): δ 13.58 (s, 1H, COO-H), 9.40 (dd, *J* = 3.0, 1.5 Hz, 1H, pyridine-H₂), 8.72 (dd, *J* = 5.0, 1.0 Hz, 1H, pyridine-H₈), 8.68 (dd, *J* = 5.0, 1.5 Hz, 1H, pyridine-H₄), 8.31 (dd, *J* = 8.0, 1.5 Hz, 1H, pyridine-H₆), 7.53-7.48 (m, 2H, pyridine-H_{3,7}), 4.82 (s, 2H, CH₂). MS (ESI) calcd for C₁₆H₉N₃O₃S₂: 355.01, found: 356.0 (M+H⁺).

5.1.2.2. *5-(5H-cyclopenta[2,1-b:3,4-b']dipyridin-5-ylidene)-2-thioxo-3-((5-(p-tolyl)-1,3,4-oxadiazol-2-yl)methyl)thiazolidin-4-one (16a)*

Yellow solid; yield: 64%; m.p.: 262–264 °C; purity by HPLC: 98.1%. ¹H NMR (DMSO-*d*₆, 500 MHz, ppm): δ 9.47 (dd, *J* = 8.5, 1.5 Hz, 1H, pyridine-H₂), 8.75 (dd, *J* = 5.0, 1.0 Hz, 1H, pyridine-H₈), 8.71 (dd, *J* = 5.0, 1.0 Hz, 1H, pyridine-H₄), 8.39 (dd, *J* = 8.0, 1.0 Hz, 1H, pyridine-H₆), 7.86 (d, *J* = 8.0 Hz, 2H, benzene-H), 7.57-7.52 (m, 2H, pyridine-H_{3,7}), 7.40 (dd, *J* = 8.0, 2.0 Hz, 2H, benzene-H), 5.63 (s, 2H, CH₂), 2.38 (s, 3H, CH₃). MS (ESI) calcd for C₂₄H₁₅N₅O₂S₂: 469.07, found: 470.3 (M+H⁺).

5.1.2.3. *3-((5-(4-Chlorophenyl)-1,3,4-oxadiazol-2-yl)methyl)-5-(5H-cyclopenta[2,1-b:3,4-b']dipyridin-5-ylidene)-2-thioxothiazolidin-4-one (16b)*

Yellow solid; yield: 66%; m.p.: 286–288 °C; purity by HPLC: 98.4%. ¹H NMR (DMSO-*d*₆, 500 MHz, ppm): δ 9.48 (dd, *J* = 6.0, 3.0 Hz, 1H, pyridine-H₂), 8.75 (dd, *J* = 4.5, 0.5 Hz, 1H, pyridine-H₈), 8.72 (dd, *J* = 5.0, 1.0 Hz, 1H, pyridine-H₄), 8.41 (d, *J* = 8.0 Hz, 1H, pyridine-H₆), 7.98 (d, *J* = 8.5 Hz, 2H, benzene-H), 7.68 (d, *J* = 8.0 Hz, 2H, benzene-H), 7.58-7.53 (m, 2H, pyridine-H_{3,7}), 5.65 (s, 2H, CH₂). MS (ESI) calcd for C₂₃H₁₂ClN₅O₂S₂: 489.01, found: 490.0 (M+H⁺).

5.1.2.4. *3-((5-(4-Bromophenyl)-1,3,4-oxadiazol-2-yl)methyl)-5-(5H-cyclopenta[2,1-b:3,4-b']dipyridin-5-ylidene)-2-thioxothiazolidin-4-one (16c)*

Yellow solid; yield: 65%; m.p.: 288–290 °C; purity by HPLC: 98.6%. ¹H NMR (DMSO-*d*₆, 500 MHz, ppm): δ 9.48 (dd, *J* = 8.5, 1.5 Hz, 1H, pyridine-H₂), 8.75 (dd, *J* = 5.0, 1.5 Hz, 1H, pyridine-H₈), 8.72 (dd, *J* = 5.0, 1.5 Hz, 1H, pyridine-H₄), 8.40 (dd, *J* = 8.0, 1.0 Hz, 1H, pyridine-H₆), 7.90 (dd, *J* = 6.5, 2.0 Hz, 2H, benzene-H), 7.82 (dd, *J* = 7.0, 2.0 Hz, 2H, benzene-H), 7.58-7.53 (m, 2H, pyridine-H_{3,7}), 5.64 (s, 2H, CH₂). MS (ESI) calcd for C₂₃H₁₂BrN₅O₂S₂: 532.96, found: 534.2

(M+H⁺).

5.2. Cytotoxicity assay

The in vitro cytotoxicity of novel compounds **11–16** was evaluated by Cell Counting Kit-8 assay (CCK-8) (DOJINDO, Kumamoto, Japan) [74] on A549 cells (human lung adenocarcinoma cell line), HepG2 cells (human gastric adenocarcinoma cell line), MCF-7 cells (human breast adenocarcinoma cell line and MRC-5 cells (human fetal lung fibroblast cell line) as a control. Cisplatin was used as a positive control. Initially, cells were routinely cultured in RPMI 1640 (Invitrogen Gibco) supplemented with 10% FBS (Invitrogen Gibco) and penicillin-streptomycin (Sigma-Aldrich, 100 U/mL) at 37.0 °C in a humidified atmosphere containing 5% CO₂. Moreover, 95 µL cell suspensions were seeded at 5000 cells per well in 96 well plates for 24 hours to culture. After that, 5 µL of a solution of compounds (1 µL of a solution of compounds in DMSO was diluted with 4 µL culture medium) was mixed into the 96 well plates sequentially to culture for 36 hours. Then 10 µL CCK-8 reagents were added to each well and incubated at 37 °C for 1 h. Finally, the optical density of each sample was measured at 450 nm using a microplate reader (Molecular Devices M4).

5.3. Electrophoretic mobility shift assay (EMSA) [24, 39]

DNA samples were prepared in a buffer (pH 7.4) containing 10 mM Tris-HCl, 10 mM KCl, 0.1 mM EDTA in the presence and absence of compounds were incubated at 4 °C for 24 h after annealing from 95 °C to r.t. EMSA was conducted using 16% native polyacrylamide gel electrophoresis and 1 × TBE (Tris base-boric acid-EDTA) buffer solution. The gels were run at 120 V for 4 h in 4 °C circulating cooling water system. The gels were then immersed in 1 × SYBR Gold and in 1 × TE solution for 30 min, respectively, rinsed with ultrapure water, and then photographed using a Bio-Rad gel imaging analyzer.

5.4. UV melting assay

According to our previous work [24,39], to measure T_m 's of examined DNA's in the presence/absence of novel 4,5-diazafluorene derivatives, UV melting assay was performed on a UV-2550 spectrophotometer (Shimadzu) equipped with a thermoelectrically controlled cell holder and quartz cells with a path length of 10 mm. In brief, The absorbance at 295 nm for 2 µM

G-rich DNAs in a buffer (pH 7.4) containing 10 mM Tris-HCl, 10 mM KCl, 0.1 mM EDTA, in the presence/absence of compounds at the increasing compound concentrations of 0, 2, 4, 8 μ M was monitored with the increasing temperatures ranging from 1 $^{\circ}$ C to 95 $^{\circ}$ C.

5.5. Circular dichroism (CD) spectroscopy assay

A Jasco J-815 Circular Dichroism (CD) spectropolarimeter was used for CD assay [39]. In brief, spectra were baseline-corrected and the signal contributions of the buffer were subtracted. Each titration data was obtained by scanning from 450 to 220 nm with a 5 mm path length quartz cuvette, averaged from at least three successive accumulations at a scan rate of 100 nm/min by using a bandwidth of 5.0 nm at a standard sensitivity. At first, DNA solutions and compound solutions alone, respectively, were scanned under the determined conditions. Then each examined compound was titrated into the same cuvette at the selected increasing concentration ratios, and the obtained complexes equilibrated after each titration for 15 min and scanned. All experiments were performed at 25 $^{\circ}$ C in a buffer (pH 7.4) containing 10 mM Tris-HCl, 10 mM KCl, 0.1 mM EDTA, and samples of 4 μ M G-rich DNA and Mut-DNA (in single strand) and 2 μ M double-stranded DNA (in double strand) dissolved in the buffer were incubated for 24 h at 4 $^{\circ}$ C after annealing at 95 $^{\circ}$ C.

5.6. Surface plasmon resonance (SPR) assay

All SPR experiments were performed on a Biacore X100 instrument with a sensor chip SA in Tris buffer (10 mM Tris-HCl, pH 7.4, 10 mM KCl, 0.1 mM EDTA, 0.005% surfactant P20) with 0.5% DMSO (v/v) at 25 $^{\circ}$ C according to our previous studies [54,55]. In brief, the sensor chip SA was preconditioned to remove any unbound streptavidin from the surface of the sensor chip with a solution of 1 M NaCl/50 mM NaOH and allowing the buffer to run for 10 min to remove any trace of NaOH until the baseline was stable. Then, two annealed 5'-biotin-TTAGGGTTAGGGTTAGGGTTAGGGTT-3' (5'-biotin-G-rich DNA), 5'-biotin-TTAGCGTTAGCGTTAGCGTTAGCGTT-3' and 5'-biotin-(TTAGGG)₄TT-TATA-AA(CCCTAA)₄-3' (5'-biotin-ds-DNA) were noncovalently immobilized on a sensor chip SA by biotin-streptavidin recognition interaction to obtain the appropriate DNA immobilization level. Finally, several serial dilutions of compound were injected at a flow rate of 20 μ L min⁻¹ in order

of increasing concentration and the equilibrium response determined relative to the baseline, association rate constant ($k_a/M^{-1}s^{-1}$), dissociation rate constant (k_d/s^{-1}), association equilibrium constant (K_A, M^{-1}) and stoichiometry were obtained by fitting the resulting sensorgrams to a theoretical model, a global 1:1 interaction model with a mass transfer effect, with the BIAevaluation 4.1 program (Bia-core/GE Healthcare), providing the affinity and specificity of binding for the compounds against 26nt telomeric G-rich DNA, Mut-DNA and ds-DNA.

5.7. Telomerase activity assay

Based on our previous study [39], the telomerase activity in A549 cells was detected by TRAPEZE® Telomerase Detection Kit (S7700-KIT; Millipore Company, Purchase, NY) according to the manufacturer's instructions, also named Trap assay. In brief, 10^6 cells was resuspended in 200 μ L of $1 \times$ CHAPS lysis buffer and incubated on ice for 30 minutes. Next, the same operation for the positive control cell pellet was completed and all supernatant transferred into a fresh tube, and protein concentration determined with BCA kit (Beyotime). 10–750 ng/ μ L protein in cell extract was incubated with TRAP buffer (20 mM Tris-HCl, pH 8.3, containing 1.5 mM $MgCl_2$, 63 mM KCl, 0.05% (v/v) Tween 20, 1 mM EGTA, and 0.01% BSA) supplemented with dNTP mix, TS primer, TRAP primer mix, ddH₂O, Taq polymerase (Takara) and compounds at used concentrations. Telomerase elongation step was conducted at 30 °C for 30 min, 95 °C for 2 min and PCR was performed at 94 °C for 15 s, 59 °C for 30 s, 72 °C for 1 min for 34 cycles and 72 °C for 5 min in a thermocycler (Bioer). PCR samples were separated on a 10% (w/v) native-PAGE gel in $0.5 \times$ TBE for 3 h at 110 V. After electrophoresis, the gel was stained with SYBR GOLD for 30 min at room temperature.

5.8. Wound healing assay

Wound healing assay was accomplished for four cancer cells A549, AGS, HepG2 and MCF-7 cells in the presence/absence of 4,5-diazafluorene derivatives **14a–c** according to published literature [24,39]. In brief, all tested cells were respectively grown in DMEM medium containing growth factors at the cell density of 1×10^5 cells/mL for 24 h. Afterwards, the monolayer of cells was scratched in a streaking motion to create an empty space with plastic pipette tip, sequentially the streaked cells were cultured in serum-free medium for an additional 28 h and photographed.

To quantify the experimental results, the % cell inhibitory rate was calculated by the equation: cell inhibitory rate (%) = $(1 - D_{\text{drug}}/D_{\text{control}}) \times 100\%$ [75], where D_{drug} is mean distance of cell migration in drug group, D_{control} is mean distance of cell migration in control group, with pictures of the initial wounded monolayers being compared with the corresponding pictures of cells at the end of the incubation.

Statistical analysis. The statistical significance of experimental results was evaluated using unpaired Student's t-tests or one-way ANOVA analysis. Data were expressed as means \pm standard deviations (S.D.) of three independent experiments and the difference ($P < 0.05$) was considered significant.

Acknowledgment

This work was supported by The National Natural Science Foundation of China (No. 21572207, 2015; No. 21877101, 2018, No. 31500739, 2015).

References

- [1] F. Bray, J. Ferlay, S. Isabelle, R.L. Siegel, L.A. Torre, A. Jemal, Global cancer statistics 2018: GLOBOCAN estimates of incidence and mortality worldwide for 36 cancers in 185 countries, *CA. Cancer J.Clin.* 68 (2018) 394–424. doi: 10.3322/caac.21492.
- [2] R. Siegel, D. Naishadham, A. Jemal, Cancer statistics, *CA. Cancer J. Clin.* 63 (2013) 11–30. doi: 10.3322/caac.21166.
- [3] J.M. Varlotto, L.N. Medford-Davis, A. Recht, J.C. Flickinger, E. Schaefer, M.M. DeCamp, Failure rates and patterns of recurrence in patients with respected N1 non-small-cell lung cancer, *Int. J. Rad. Onc. Biol. Phys.* 81 (2011) 353–359. doi: 10.1016/j.ijrobp.2010.05.022.
- [4] P. Saintigny, J.A. Burger, Recent advances in non-small cell lung cancer biology and clinical management, *Discov. Med.* 13 (2012) 287–297. doi: 10.1186/1479-5876-10-68.
- [5] N. van Zandwijk, Neoadjuvant strategies for non-small cell lung cancer, *Lung Cancer.* 34 (2001) 145-150. doi: 10.1016/s0169-5002(01)00359-2.
- [6] C.C. Schneider, R. Archid, N. Fischer, S. Bühler, S. Venturelli, A. Berger, M. Burkard, A. Kirschniak, R. Bachmann, A. Königsrainer, J. Glatzle, D. Zieker. Metabolic alteration-Overcoming therapy resistance in gastric cancer via PGK-1 inhibition in a combined therapy

- with standard chemotherapeutics, *Int. J. Surg.* 22 (2015) 92–98. doi: 10.1016/j.ijso.2015.08.020.
- [7] V.G.M. Naidu, B.U. Mahesh, A.K. Giddam, K.R.D. Babu, J Ding, K.S. Babu, B. Ramesh, R.R. Pragada, P. Gopalakrishnakone, Apoptogenic activity of ethyl acetate extract of leaves of *Memecylonedule* on human gastric carcinoma cells via mitochondrial dependent pathway, *Asian Pac J Trop Med* 6 (2013) 337–345. doi: 10.1016/S1995-7645(13)60036-X.
- [8] X.F. Yuan, Q. Zhang, Z.Z. Li, X.L. Zhang, S.Q. Bao, D.M. Fan, Y.G. Ru, S.X. Dong, Y.Z. Zhang, Y.J. Zhang, Z. Ye, D.S. Xiong, Mesenchymal stem cells deliver and release conditionally replicative adenovirus depending on hepatic differentiation to eliminate hepatocellular carcinoma cells specifically, *Cancer Lett.* 381 (2016) 85–95. doi: 10.1016/j.canlet.2016.07.019.
- [9] D.E. Gomez, R.G. Armando, H.G. Farina, P.L. Menna, C.S. Cerrudo, P.D. Ghiringhelli, D.F. Alonso, Telomere structure and telomerase in health and disease, *Int. J. Oncol.* 41 (2012) 1561–1569. doi: 10.3892/ijo.2012.1611.
- [10] D.L.M. Gómez, H.G. Farina, D.E. Gómez, Telomerase regulation: A key to inhibition, *Int. J. Oncol.* 43 (2013) 1351–1356. doi: 10.3892/ijo.2013.2104.
- [11] X.B. Sui, N. Kong, Z.G. Wang, H.M. Pan, Epigenetic regulation of the human telomerase reverse transcriptase gene: A potential therapeutic target for the treatment of leukemia, *Oncol. Lett.* 6 (2013) 317–322. doi: 10.3892/ol.2013.1367.
- [12] W.B. Chen, L.J. Qin, S.S. Wang, M. Li, D.B. Shi, Y. Tian, J.S. Wang, L.Y. Fu, Z.L. Li, W. Guo, W.D. Yu, Y.H. Yuan, T.B. Kang, W.L. Huang, W.G. Deng, CPSF4 activates telomerase reverse transcriptase and predicts poor prognosis in human lung adenocarcinomas, *Mol. Oncol.* 8 (2014) 704–716. doi: 10.1016/j.molonc.2014.02.001.
- [13] Y.J. Park, E.K. Kim, J.Y. Bae, S. Moon, J. Kim, Human telomerase reverse transcriptase (hTERT) promotes cancer invasion by modulating cathepsin D via early growth response (EGR)-1, *Cancer Lett.* 370 (2016) 222–231. doi: 10.1016/j.canlet.2015.10.021.
- [14] R.K. Moyzis, J.M. Buckingham, L.S. Cram, M. Dani, L.L. Deaven, M.D. Jones, J. Meyne, R.L. Ratliff, J.R. Wu, A highly conserved repetitive DNA-sequence, (ttaggg)_n, present at the telomeres of human-chromosomes, *Proc. Nat. Acad. Sci. U.S.A.* 85 (1988) 6622–6626. doi: 10.2307/32432.

- [15] J.A. Zhou, G. Yuan, Specific recognition of human telomeric G-quadruplex DNA with small molecules and the conformational analysis by esi mass spectrometry and circular dichroism spectropolarimetry, *Chem. Eur. J.* 13 (2007) 5018–5023. doi:10.1002/chem.200601605.
- [16] S. Neidle, Human telomeric G-quadruplex: the current status of telomeric G-quadruplexes as therapeutic targets in human cancer, *FEBS. J.* 277 (2010) 1118–1125. doi: 10.1111/j.1742-4658.2009.07463.x.
- [17] A. Bugaut, P. Alberti, Understanding the stability of DNA G-quadruplex units in long human telomeric strands, *Biochimie.* 113 (2015) 125–133. doi: 10.1016/j.biochi.2015.04.003.
- [18] K. Nalapareddy, H. Jiang, L.M.G. Gutierrez, K.L. Rudolph, Determining the influence of telomere dysfunction and DNA damage on stem and progenitor cell aging—what markers can we use? *Exp. Gerontol.* 43 (2008) 998–1004. doi: 10.1016/j.exger.2008.09.002.
- [19] S. Maiti, P. Saha, T. Das, I. Bessi, H. Schwalbe, J. Dash. Human telomeric G-quadruplex selective fluoro-isoquinolines induce apoptosis in cancer cells. *Bioconjugate Chemistry.* 29 (2018), 1141–1154. doi: 10.1021/acs.bioconjchem.7b00781.
- [20] T. Che, S.B. Chen, J.L. Tu, B. Wang, Y.Q. Wang, Y. Zhang, J. Wang, Z.Q. Wang, Z.P. Zhang, T.M. Ou, Y. Zhao, J.H. Tan, Z.S. Huang, Discovery of novel schizocommunin derivatives as telomeric G-quadruplex ligands that trigger telomere dysfunction and the deoxyribonucleic acid (DNA) damage response, *J. Med. Chem.* 61 (2018) 3436–3453. doi:10.1021 / acs.jmedchem.7b01615.
- [21] S. Manna, D. Sarkar, S.G. Srivatsan, A dual-app Nucleoside probe provides structural insights into the human telomeric overhang in live cells, *J. Am. Chem. Soc.* 140 (2018) 12622–12633. doi: 10.1021/jacs.8b08436.
- [22] M. Wang, W. Wang, T.S. Kang, C.H. Leung, D.L. Ma, Development of an iridium(III) complex as a G-quadruplex probe and its application for the G-quadruplex-based luminescent detection of picomolar insulin. *Anal. Chem.* 88 (2015) 981–987. doi: 10.1021/acs.analchem.5b04064.
- [23] X.C. Chen, S.B. Chen, J. Dai, J.H. Yuan, T.M. Ou, Z.S. Huang, J.H. Tan, Tracking the dynamic folding and unfolding of RNA G-quadruplexes in live cells. *Angew. Chem.* 57 (2018) 4702–4706. doi:10.1002/anie.201801999.
- [24] J.C. Liu, M. Chen, Y.L. Wang, X.Y. Zhao, S.J. Wang, Y.L. Wu, W. Zhang. Synthesis and the

- interaction of 2-(1H-pyrazol-4-yl)-1H-imidazo[4,5-f][1,10]phenanthrolines with telomeric DNA as lung cancer inhibitors, *Euro. J. Med. Chem.* 133 (2017) 36–49.,doi: 10.1016/j.ejmech.2017.03.030.
- [25] Y.C. Lin, Y.F. Chen, L.S. Tseng, Y.H. Lee, S.L. Morris-Natschke, S.C. Kuo, N.S. Yang, K.H. Lee, L.J. Huang, Synthesis and structure-activity relationship studies of novel 3,9-substituted α -carboline derivatives with high cytotoxic activity against colorectal cancer cells, *Eur. J. Med. Chem.* 110 (2016) 98–114.,doi: 10.1016/j.ejmech.2016.01.004.
- [26] M.X. Song, C.J. Zheng, X.Q. Deng, Q. Wang, S.P. Hou, T.T. Liu, X.L. Xing, H.R. Piao, Synthesis and bioactivity evaluation of rhodanine derivatives as potential anti-bacterial agents, *Eur. J. Med. Chem.* 54 (2012) 403–412. doi: 10.1016/j.ejmech.2012.05.023.
- [27] S.B. Jiang, S.R. Tala, H. Lu, N.E. Abo-Dya, I. Avan, K. Gyanda, L. Lu, A.R. Katritzky, A.K. Debnath, Design, Synthesis, and Biological Activity of Novel 5-((Arylfuran/1H-pyrrol-2-yl)methylene)-2-thioxo-3-(3-(trifluoromethyl)- phenyl)thiazolidin-4-ones as HIV-1 Fusion Inhibitors Targeting gp41, *J. Med. Chem.* 54 (2011) 572–579. doi: 10.1021/jm101014v.
- [28] S. Ravi, K.K. Chiruvella, K. Rajesh, V. Prabhu, S.C. Raghavan, 5-Isopropylidene-3-ethyl rhodanine induce growth inhibition followed by apoptosis in leukemia cells, *Eur. J. Med. Chem.* 45 (2010) 2748–2752. doi: 10.1016/j.ejmech.2010.02.054.
- [29] R. Ottanà, P. Paoli, A. Naß, G. Lori, V. Cardile, I. Adornato, A. Rotondo, A.C.E. Graziano, G. Wolber, R. Maccari, Discovery of 4-[(5-arylidene-4-oxothiazolidin-3-yl)methyl]benzoic acid derivatives active as novel potent allosteric inhibitors of protein tyrosine phosphatase 1B: In silico studies and in vitro evaluation as insulinomimetic and anti-inflammatory agents, *Eur. J. Med. Chem.* 127 (2017) 840–858. doi: 10.1016/j.ejmech.2016.10.063.
- [30] B.T. Moorthy, S. Ravi, M. Srivastava, K.K. Chiruvella, H. Hemlal, O. Joy, S.C. Raghavan, Novel rhodanine derivatives induce growth inhibition followed by apoptosis. *Bioorg. Med. Chem. Lett.* 20 (2010) 6297–6301. doi: 10.1016/j.bmcl.2010.08.084.
- [31] J.J. Zhao, X.F. Wang, B.L. Li, R.L. Zhang, B. Li, Y.M. Liu, C.W. Li, J.B. Liu, B.Q. Chen, Synthesis and in vitro antiproliferative evaluation of novel nonsymmetrical disulfides bearing 1,3,4-oxadiazole moiety, *Bioorg. Med. Chem. Lett.* 26 (2016) 4414–4416. doi: 10.1016/j.bmcl.2016.08.014.
- [32] M.J. Plater, S. Kemp, E. Lattmann, Heterocyclic free radicals. Part 1. 4,5-Diazafluorene

- derivatives of Koelsch's free radical: an EPR and metal-ion complexation study, *J. Chem. Soc. Perkin Trans. 1* (2000) 971–979. doi:10.1002/chin.200028148.
- [33] G. Nocton, C.H. Booth, L. Maron, R.A. Andersen, Thermal Dihydrogen Elimination from Cp*₂Yb(4,5-diazafluorene), *Organometallics* 32 (2013) 1150–1158. doi:10.1021/om300876b.
- [34] J.C. Liu, C.J. Zheng, M.X. Wang, Y.R. Li, L.X. Ma, S.P. Hou, H.R. Piao, Synthesis and evaluation of the antimicrobial activities of 3-((5-phenyl-1,3,4-oxadiazol-2-yl)methyl)-2-thioxothiazolidin-4-one derivatives, *Eur. J. Med. Chem.* 74 (2014) 405–410. doi:10.1016/j.ejmech.2013.12.054.
- [35] L. Ying, J.J. Green, H. Li, D. Klenerman, S. Balasubramanian, Studies on the structure and dynamics of the human telomeric G-quadruplex by single-molecule fluorescence resonance energy transfer, *Proc. Natl. Acad. Sci. USA.* 100 (2003) 14629–14634. doi:10.1073/pnas.2433350100.
- [36] J.X. Dai, M. Carver, D.Z. Yang, Polymorphism of human telomeric quadruplex structures. *Biochimie* 90 (2008) 1172–1183. doi:10.1016/j.biochi.2008.02.026.
- [37] R. De Armond, S. Wood, D. Sun, L.H. Hurley, S.W. Ebbinghaus, Evidence for the presence of a guanine quadruplex forming region within a polypurine tract of the hypoxia inducible factor 1 α promoter, *Biochemistry* 44 (2005) 16341–16350. doi:10.1021/bi051618u.
- [38] I. M. Pedroso, L.F. Duarte, G. Yanez, K. Burkewitz, T. M. Fletcher, Sequence specificity of inter- and intramolecular G-quadruplex formation by human telomeric DNA, *Biopolymers* 87 (2007) 74–84. doi:10.1002/bip.20790.
- [39] W. Zhang, M. Chen, Y.L. Wu, Y. Tanaka, Y.J. Ji, S.L. Zhang, C.H. Wei, Y. Xu, Formation and stabilization of the telomeric antiparallel G-quadruplex and inhibition of telomerase by novel benzothioxanthene derivatives with anti-tumor activity, *Sci. Rep.* 2015, doi:10.1038/srep13693.
- [40] M. Vorlíčková, J. Chládková, I. Kejnovská, M. Fialová, J. Kypr, Guanine tetraplex topology of human telomere DNA is governed by the number of (TTAGGG) repeats, *Nucl. Acids Res.* 33 (2005) 5851–5860. doi:10.1093/nar/gki898.
- [41] H.Q. Yu, D. Miyoshi, N. Sugimoto, Characterization of structure and stability of long telomeric DNA G-quadruplexes, *J. Am. Chem. Soc.* 128 (2006) 15461–15468. doi:

10.1021/ja064536h.

- [42] A. Siddiqui-Jain, C.L. Grand, D.J. Bearss, L.H. Hurley, Direct evidence for a G-quadruplex in a promoter region and its targeting with a small molecule to repress c-MYC transcription, *Proc. Natl. Acad. Sci.* 99 (2002) 11593–11598. doi:10.1073/pnas.182256799.
- [43] T.M. Ou, C. Zhang, Z.S. Huang, X.D. Wang, J.H. Tan, Y. Chen, D.L. Ma, K.Y. Wong, J.C.O. Tang, A.S.C. Chan, L.Q. Gu, Stabilization of G-Quadruplex DNA and Down-Regulation of Oncogene c-myc by Quindoline Derivatives, *J. Med. Chem.* 50 (2007) 1465–1474. doi.org/10.1021/jm0610088.
- [44] J.L. Mergny, A.T. Phan, L. Lacroix, Following G-quartet formation by UV-spectroscopy, *FEBS Lett.* 435 (1998) 74–78. doi:10.1016/S0014-5793(98)01043-6.
- [45] P.A. Rachwal, K.R. Fox, Quadruplex melting, *Methods* 43 (2007) 291–301. doi:10.1016/j.ymeth.2007.05.004.
- [46] L. Ying, J.J. Green, H. Li, D. Klenerman, S. Balasubramanian, Studies on the structure and dynamics of the human telomeric G-quadruplex by single-molecule fluorescence resonance energy transfer, *Proc. Natl. Acad. Sci. USA.* 100 (2003) 14629–14634. doi:10.1073/pnas.2433350100.
- [47] A.T. Phan, J.L. Mergny, Humantelomeric DNA: G-quadruplex, i-motif and Watson-Crick double helix, *Nucl. Acids Res.* 30 (2002) 4618–4625. doi:10.1093/nar/gkf597.
- [48] J. Kypr, I. Kejnovská, D. Renciuk, M. Vorlíčková, Circular dichroism and conformational polymorphism of DNA. *Nucl. Acids Res.* 37 (2009) 1713–1725. doi: 10.1093/nar/gkp026.
- [49] M. Vorlíčková, I. Kejnovská, J. Sagi, D. Renčiuk, K. Bednářová, J. Motlová, J. Kypr, Circular dichroism and guanine quadruplexes. *Methods* 57 (2012) 64–75. doi: 10.1016/j.ymeth.2012.03.011. M. Vorlíčková, I. Kejnovská,
- [50] A. Ambrus, D. Chen, J. Dai, T. Bialis, R.A. Jones, D. Yang, Human telomeric sequence forms a hybrid-type intramolecular G-quadruplex structure with mixed parallel/antiparallel strands in potassium solution. *Nucl. Acids Res.* 34 (2006) 2723–2735. doi: 10.1093/nar/gkl348
- [51] A. Matsugami, Y. Xu, Y. Noguchi, H. Sugiyama, M. Katahira, Structure of a human telomeric DNA sequence stabilized by 8-bromoguanosine substitutions, as determined by NMR in a K⁺ solution, *FEBS J.* 274 (2007) 3545–3556. Doi:10.1111/j.1742-

4658.2007.05881.x

- [52] I.N. Rujan, J.C. Meleney, P.H. Bolton, Vertebrate telomere repeat DNAs favor external loop propeller quadruplex structures in the presence of high concentrations of potassium, *Nucl Acids Res.* 33 (2005) 2022–2031. doi:10.1093/nar/gki345.
- [53] W. Li, P. Wu, T. Ohmichi, N. Sugimoto, Characterization and thermodynamic properties of quadruplex/duplex competition. *FEBS Lett.* 526 (2002) 77–81. doi: 10.1016/S0014-5793(02)03118-6.
- [54] W. Zhang, T. Bando, H. Sugiyama, Discrimination of hairpin polyamides with an alpha-substituted-gamma-aminobutyric acid as a TG-reader in DNA minor groove, *J. Am. Chem. Soc.* 128 (2006) 8766–8776. doi:10.1021/ja0580587.
- [55] W. Zhang, S.K. Jiang, Y.L. Wu., C.X. Guo, H.F. Zhang, H. Sugiyama, X.L. Chen, Discrimination between T/A and A/T base pairs of pyrrole-imidazole polyamides substituted with chiral β -hydroxy- γ -aminobutyric acid/ β -alanine pairs, *CHEMBIOCHEM* 13 (2012) 47–50. doi:10.1002/cbic.201100675.
- [56] B. Nguyen, F.A. Tanious, W.D. Wilson, Biosensor-surface plasmon resonance: Quantitative analysis of small molecule–nucleic acid interactions, *Methods* 42 (2007) 150–161. doi:10.1016/j.ymeth.2006.09.009.
- [57] A.M. Whitney, S. Ladame, S. Balasubramanian, Templated ligand assembly by using G-Quadruplex DNA and dynamic covalent chemistry, *Angew Chem Int Ed Engl.* 43 (2004) 1143–1146. doi:10.1002/anie.200353069.
- [58] D.P.N. Gonçalves, R. Rodriguez, S. Balasubramanian, J.K.M. Sanders, Tetramethylpyridiniumporphyrazines—a new class of Gquadruplex inducing and stabilising ligands, *Chem Commun.* 45 (2006) 4685–4687. doi:10.1039/b611731g.
- [59] P. Wang, L.G. Ren, H.P. He, F. Liang, X. Zhou, Z. Tan, A phenol quaternary ammonium porphyrin as a potent telomerase inhibitor by selective interaction with quadruplex DNA, *ChemBioChem* 7 (2006) 1155–1159. doi:10.1002/cbic.200600036.
- [60] J.W. Shay, W.E. Wright, Telomerase: A target for cancer therapeutics, *Cancer Cell* 2 (2002) 257–265. doi:10.1016/S1535-6108(02)00159-9.
- [61] N.W. Kim, M.A. Piatyszek, K.R. Prowse, C.B. Harley, M.D. West, P.L. Ho, G.M. Coviello, W.E. Wright, S.L. Weinrich, J.W. Shay, Specific Association of human telomerase activity

- with immortal cells and cancer, *Science* 266 (1994) 2011–2015. doi:10.1126/science.7605428.
- [62] R. Hannen, J. W. Bartsch, Essential roles of telomerase reverse transcriptase hTERT in cancer stemness and metastasis, *FEBS Lett.* 592 (2018) 2023–2031. doi: 10.1002/1873-3468.13084.
- [63] W.M. Kong, N.N. Lv, W.Y. Z. Wysham, D.R. Roque, T.Q. Zhang, S.M. Jiao, D. Song, J. Chen, V.L. Bae-Jump, C.X. Zhou. Knockdown of hTERT and Treatment with BIBR1532 Inhibit Cell Proliferation and Invasion in Endometrial Cancer Cells, *Cancer* 6 (2015) 1337–1345. doi: 10.7150/jca.13054.eCollection 2015.
- [64] P. Murat, Y. Singh, E. Defrancq, Methods for investigating G-quadruplex DNA/ligand interactions, *Chem. Soc. Rev.* 40 (2011) 5293–5307. doi: 10.1039/c1cs15117g.
- [65] G. Raju, R. Srinivas, V.S. Reddy, M.M. Idris, A. Kamal, N. Nagesh, Interaction of pyrrolobenzodiazepine (PBD) ligands with parallel intermolecular G-quadruplex complex using spectroscopy and ESI-MS, *PLoS ONE* 7 (2012) e35920. doi:10.1371/journal.pone.0035920.
- [66] A.M. Zahler, J.R. Williamson, T.R. Cech, D.M. Prescott, Inhibition of telomerase by G-quartet DNA structures, *Nature* 350 (1991) 718–20. doi:10.1038/350718a0.
- [67] M.H. Hu, S.B. Chen, B. Wang, T.M. Ou, L.Q. Gu, J.H. Tan, Z.S. Huang, Specific targeting of telomeric multimeric G-quadruplexes by a new triaryl-substituted imidazole. *Nucl. Acids Res.* 45 (2017) 1606–1618. doi:10.1093/nar/gkw1195.
- [68] L. Oganessian, T.M. Bryan, Physiological relevance of telomeric G-quadruplex formation: A potential drug target, *Bioessays* 29 (2007) 155–165. doi:10.1002/bies.20523.
- [69] X.H. Zheng, G. Mu, Y.F. Zhong, T.P. Zhang, Q. Cao, L.N. Ji, Y. Zhao, Z.W. Mao, Trigeminal star-like platinum complexes induce cancer cell senescence through quadruplex-mediated telomere dysfunction. *Chem. Commun.* 52 (2016) 14101–14104. doi: 10.1039/C6CC08254H.
- [70] E.M. Rezler, D.J. Bearss, L.H. Hurley, Telomeres and telomerases as drug targets, *Curr. Opin. Pharmacol.* 2 (2002) 415–423. doi:10.1016/S1471-4892(02)00182-0.
- [71] S. Neidle, G.N. Parkinson, Telomere maintenance as a target for anticancer drug discovery, *Nat. Rev. Drug Discov.* 1 (2002) 383–393. doi:10.1038/nrd793.

- [72] A. De Cian, L. Lacroix, C. Douarre, N. Temime-Smaali, C. Trentesaux, J.F. Riou, J.L. Mergny, Targeting telomeres and telomerase, *Biochimie* 90 (2008) 131–155. doi:10.1016/j.biochi.2007.07.011.
- [73] M.K. Islam, P.J. Jackson, K.M. Rahman, D.E. Thurston, Recent advances in targeting the telomeric G-quadruplex DNA sequence with small molecules as a strategy for anticancer therapies. *Future Med. Chem.* 8 (2016) 1259–1290. doi: 10.4155/fmc-2015-0017.
- [74] Y. Yan, J. Tan, T. Ou, Z. Huang, L. Gu, DNA G-quadruplex binders: a patent review, *Expert Opin. Ther. Pat.* 23 (2013) 1495–1509. doi: 10.1517/13543776.2013.833187.
- [75] C. C. Thompson, F.J. Ashcroft, S. Patel, G. Saraga, D. Vimalachandran, W. Prime, F. Campbell, A. Dodson, R.E. Jenkins, N.R. Lemoine, T. Crnogorac-Jurcevic, H.L. Yin, E. Costello, Pancreatic cancer cells overexpress gelsolin family-capping proteins, which contribute to their cell motility, *Gut*. 56 (2007) 95–106. doi:10.1136/gut.2005.083691.

Highlights:

>19 novel 4,5-diazafluorene derivatives were synthesized.

>**14c** showed strongest inhibitory activity with an IC_{50} value of 1.13 μ M and an SI value of 7.01 relative to MRC-5 cells against A549 cell line.

>4,5-diazafluorene derivatives could stabilize telomeric G-quadruplexes and consequently inhibit telomerase activity.

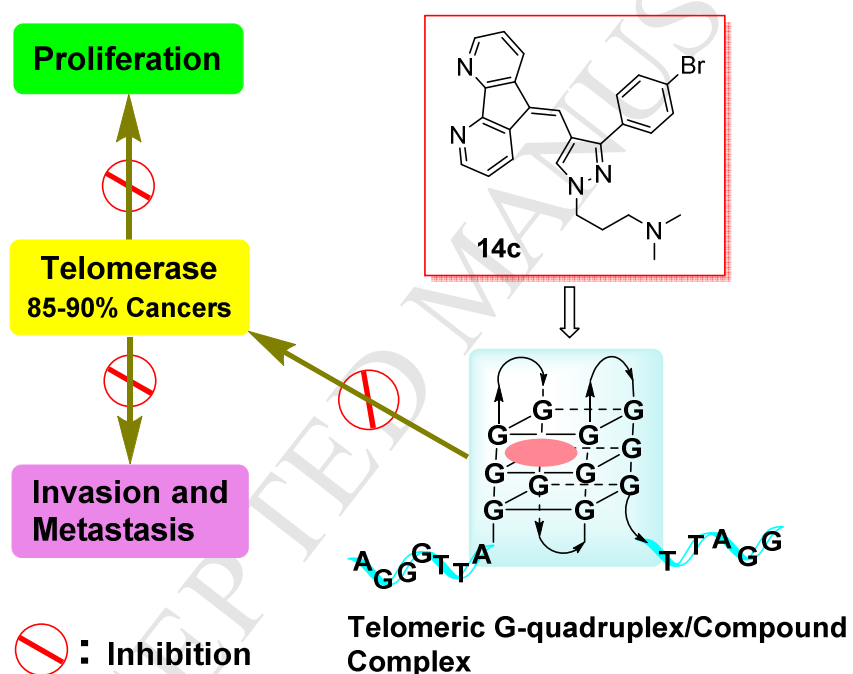
Graphical Abstract:

Figure captions:

Fig. 1. The effects of telomerase on the proliferation, invasion and metastasis of cancer cells and development of telomerase targeted drugs mediated by formation and stabilization of DNA G-quadruplex.

Fig. 2. Viability of A549 cells treated with 10 μM of compounds **11–16** (A), and A549 cells (B), AGS cells (C), HepG2 cells (D), MCF-7 cells (E), and MRC-5 cells (F) treated with compounds **14a-c** with 0, 1, 2, 4, 8 and 16 μM for 36 h, respectively. Cell viability was determined using Cell Counting Kit-8 assay. Cisplatin: positive control; 1% DMSO is 1% DMSO solution in RPMI 1640 as a reference.

Fig. 3. The ability of four 4,5-diazafluorene derivatives **14a–c** and **16c** to promote the formation of G4-DNA structures by EMSA in a 26nt telomeric single-stranded DNA sequence (G-rich DNA). Lane 1: DNA Marker alone; Lane 2: G-rich DNA alone in 1% DMSO containing buffer; Lane 3-6: G-rich DNA + compound **16c**; Lane 7-10: G-rich DNA + compound **14a**; Lane 11-14: G-rich DNA + compound **14b**; Lane 15-18: G-rich DNA + compound **14c**. Final concentration of DNA's is 2 μM for single-stranded DNA (in single strand); the increasing concentration of each compound is 1.5, 3, 6 and 12 μM from left to right.

Fig. 4. The ability of 4,5-diazafluorene derivatives to specifically interact with G-quadruplex structures formed in a 26nt telomeric single stranded DNA sequence (G-rich DNA in **Table 2**) by CD (A and B) and SPR (C). Arrows at 240-245 nm (A) and 240-241 nm (B) denote the change of negative peak of telomeric G-quadruplex with the increase of the **14C** and **16C** concentration, respectively; an arrow at 270 nm (A and B) denotes the shoulder band of a 3+1 telomeric G-quadruplex structure; arrows at 290-292 nm (A) and 290-291.5 nm (B) denote the change of positive peak of telomeric G4-DNA with the increase of the **14C** and **16C** concentration, respectively; arrows near 298.5 nm (A) and 300.5 nm (B) denote the isoelliptic points; arrows at 358 nm (A) and 377 nm (B) denote the change of ICD positive band from 309-430 nm (A) and 311-435 nm (B) with the increase of the **14C** and **16C** concentration, respectively. CD spectra for 26 nt telomeric G-rich DNA sequences of human chromosome in 10 mM K^+ by titration of the compounds at the ratio of a compound to DNA (r), 0.0, 0.25, 0.5, 1.0, 2.0, 3.0, 4.0, 5.0, 6.0 at concentrations of a compound ranging from 0.0 μM (red curve, highest positive peak for DNA alone) to 24 μM (cyan curve, lowest negative peak). All experiments were performed in a buffer (pH 7.4) containing 10 mM Tris-HCl, 10 mM KCl, 0.1 mM EDTA, and a sample of 4 μM G-rich DNA (in single strand) dissolved in the buffer was incubated for 24 h after annealing at 95 $^{\circ}\text{C}$. Red solid curve: DNA alone; red dotted line: compound alone. (C) A typical SPR sensorgram for the interaction of the **14C** with the G-quadruplex structure formed in a G-rich DNA (Table 2)

immobilized on the surface of a sensor chip SA. The binding response is changed with time. The data are globally fitted to a 1:1 interaction model with a mass transfer effect. Experimental curves are shown in color and fitting curves in black. The association phase was allowed to run for 300 sec to reach steady state and the dissociation phase for 280 sec for all concentrations used. Concentrations of the **14C** were used according to arrow direction: 6.25 (yellow), 12.5 (magenta), 25.0 (cyan), 50.0 (spring green), 100 (blue), 200 (gray), 400 (dark magenta), 600 (sky blue), 800 (sea green), and 1000 nM (dark blue, highest curve), respectively. Each experiment was carried out in triplicate.

Fig. 5. Ability of telomerase activity inhibition by compounds **14a**, **14b** and **14c**. (A) Telomerase activity inhibition mediated by compounds at the increasing concentrations, 0, 2, 4 and 8 μ M in A549 cells. The arrow presents a 36 bp internal control. (B) Telomerase activity was quantitated as the percent of the corresponding control. The mean of three independent experiments with comparable results was shown. Error bars indicate \pm SD.

Fig. 6. Effect of compounds **14a-c** on the mobility of A549 (A), AGS (B), HepG2 (C) and MCF-7 (D) cell lines. The mobility changes of A549 cells in the presence and absence of **14a-c** at the concentration of 0, 0.1, 0.2, and 0.4 μ M for 48 h, respectively. Cell inhibitory rate (%) for suppression of the migration in cancer cells as a function of concentrations of compounds **14a-c**. The % cell inhibitory rate was calculated by the equation: cell inhibitory rate (%) = $(1 - D_{\text{drug}}/D_{\text{control}}) \times 100\%$, where D_{drug} is mean distance of cell migration in drug group, D_{control} is mean distance of cell migration in control group; Values are the means \pm S.D. ($P < 0.05$).

Fig. 7. Highly occupied binding modes of compounds **14c** and **16c** with 5MVB. 5MVB is represented by its soft atom charge surface in **A**, while its backbone model is shown in **B**. Compounds **14c** and **16c** extracted from the complex are shown in **C**. **14c** is shown in yellow CPK and stick models, and **16c** is shown in blue CPK and stick models. The compound **14c** has the highest Molecular_3D_SASA (the total solvent accessible surface area) of 695.86 \AA^2 , while compound **16c** has thirty less than that of the former.

Scheme captions:

Scheme 1. Structure of the leading compounds and design strategy of the target compounds.

Scheme 2. Synthesis of 4,5-diazafluorene target compounds **11-16**.

Table captions:**Table 1.**

IC₅₀ values (μM) for the A549, AGS, HepG2, MCF-7, and MRC-5 cell lines treated with the desired compounds **14a-c** and a positive control drug (cisplatin). The values are expressed as the mean ± SD (triplicates).

Table 2.

The sequences of DNA oligomers used in this study.

Table 3.

T_m (°C) values for Tel-26nt G-rich DNA in the presence/absence of 4,5-diazafluorene derivatives **14a-c** and **16c**.

Table 4.

Binding kinetic constants of **14c** to DNA's by SPR^a.

Table 5.

The LibDock scores and docking interactions of compounds (**14a-c**, **16c**) with human telomeric DNA G-quadruplex (PDB ID: 5MVB).

- > 19 novel 4,5-diazafluorene derivatives were synthesized.
- > **14c** showed strongest inhibitory activity with an IC_{50} value of 1.13 μ M and an SI value of 7.01 relative to MRC-5 cells against A549 cell line.
- > 4,5-diazafluorene derivatives could stabilize telomeric G-quadruplexes and consequently inhibit telomerase activity.

ACCEPTED MANUSCRIPT